Modelling and control of an inverted double pendulum

Högni Þorsteinsson (s182555)

Master of Science in Engineering

2020

DTU Electrical Engineering
Department of Electrical Engineering

Modelling and control of an inverted double pendulum

Report written by:
Högni Þorsteinsson (s182555)

Advisor(s):
Hans Henrik Niemann, Associate Professor at the Electrical Engineering Department of DTU
Nils Axel Andersen, Associate Professor at the Electrical Engineering Department of DTU

DTU Electrical Engineering
Technical University of Denmark
2800 Kgs. Lyngby
Denmark

elektro@elektro.dtu.dk

Project period: 15 June- 15 November 2020

ECTS: 30

Education: M.Sc.

Field: Electrical Engineering

Class: Public

Edition: 1. edition

Remarks: This report is submitted as partial fulfillment of the requirements for graduation in the above education at the Technical University of Denmark.

Abstract

This thesis describes the process of designing and implementing a discrete controller for a nonlinear unstable system, the inverted double pendulum on a cart. The goal is to find a robust controller able to stabilize the pendulum in it's upright position. This is done with H_∞ optimisation for the system in a mixed-sensitivity setup.
For the purpose of system analysis and controller design a mathematical model is derived, describing the system dynamics. Both the uncontrolled and the closed loop system are analysed. Based on the analysis the controller design is systematically improved with respect to the project's performance specification. Results of experiments are presented and the performance of a number of different controller designs are compared and evaluated.
Although the controllers designed were able to stabilize the computer simulated system, no successful attempts were made on the real physical device. The suspected cause of this failure will be discussed and some suggestions made on how the system may be improved.

Contents

CHAPTER 1

Introduction

The inverted double pendulum on a cart is a classic control problem that deals with stabilizing an unstable nonlinear system. The system is also regarded as an under-actuated system, meaning that the system's degrees of freedom outnumber the actuators in the system. In other words the two joints of the pendulum and the cart position are to be influenced by a single motor. Stabilizing such a system is quite challenging, which in turn makes this a very interesting research case for feedback control.
As the title indicates the thesis includes mathematical modelling of the system, and finally the discrete implementation of the controller will be described.
The scope of the project might be considered quite large, but that was actually one of the main motivation for choosing this project. The project also offered the opportunity of working on a real physical system rather then only working with a computer-simulated system. Dealing with the complications introduced by a real system offers a different perspective and a very valuable practical knowledge.
In this thesis the author will describe his attempt to overcome the obstacles met, both theoretical and practical, while pursuing the goal of stabilizing the inverted double pendulum.

1.1 Background

The inverted double pendulum is not a very practical system. This system is mainly an interesting research topic since commercially there is not much use for such a device. There are of course similarities to other system. As an example the problem of stabilizing a rocket in a vertical take-off can be approached as an inverted pendulum. Also the under-actuated nature of this system also applies to many other fields such as robotics, aerial- and marine vehicle.
Through the years many control strategies have been used for solving this problem. In this project the aim is to design a robust controller through H_∞ optimisation. This type of controller started to gain interest in the 1980's due to shortcomings of LQG control with regard to robustness [SP05].
The particular device (Test-Rig) studied in this project is more then 20 years old and has been the subject for at least two projects prior to the one described in this thesis. It is safe to say that it was not in a good condition when the author first encountered the device. So as a project course at DTU's Department of Electrical Engineering the author upgraded the device such that it was operable without changing it's dynamics

drastically. The work done in that project course should not be evaluated in this thesis, how ever it is relevant to occasionally point out the differences between the upgraded system and the old system.
This project is based on the previous Masters thesis of Jesper K. Poulsen who successfully designed and implemented a stabilizing controller for the system [Pou01]. His paper will be extensively referred to especially with regards to system modelling. Poulsen based his work on the system modelling originally done for project from 1997 [Lut97].

1.2 Objectives

Since a mathematical model of the Test-Rig was available it is natural that the same model will be used as a basis for this project. That being said, improvements should be expected since some parameters of Test-Rig have most likely changed over the years. Improvement of the model are one of the project objectives.
The upgraded system and the old system differ drastically in terms of the motor subsystem, where a different amplifier. In Poulsen's successful attempt to stabilize the system he used a powerful amplifier able to deliver the energy needed for the task in a sufficiently brief time period. However, due to the big size of that amplifier, he also attempted to stabilize the system using smaller less powerful amplifier but in that case he did not succeed.
The ultimate goal of this project is to design and implement a stabilizing controller for the system that includes this small and less powerful amplifier. This goal can be divided into a number of objectives which are listed below.

- System modeling.
- Model verification.
- System analysis.
- Controller Design.
- Closed loop analysis.
- Real-time programming for controller implementation and data analysis.

Through out this thesis experiments and their results will be put forward that help validate whether these objectives have been met fully, to some extent or not at all.

1.3 Limitations

Rather then starting this project from scratch, building the pendulum-, motor- and sensor system the Test-Rig from a previous project was used. This might to some extent

be viewed as a limitation, since some design features of the Test-Rig are considered to be flawed. Also due to wear, tear and accumulated dirt in this old device, parameters have most likely deviated from original values used for mathematical modelling. Friction constants are very sensitive to dirt, also lag or delay due to slack in the drive-train might also have appeared over the years. Besides wear and dirt accumulation in joints and on surfaces, the pendulum arms have a slight offset from the vertical axis, that is they lean a little bit out of their ideal plane of motion.
Like stated above Poulsen was successful in his project, using a powerful amplifier in the motor sub-system. His attempts with a less powerful amplifier were however not successful. In this project the choice is made to use the less powerful amplifier and attempt to stabilize the system with the limited power available from this amplifier.

1.4 Thesis outline

To conclude this first chapter a brief overview of the following chapters is given here.

- **Analysis:** presents alternatives to the approach taken in this project.
- **System Modeling:** is described in this chapter. First, using Newtons´s law of motion, a model for the pendulum is derived and then a model for the motor system. These systems are combined for a full system model, both linear and non-linear. Finally the quality of the full model is addressed.
- **System Analysis:** in time domain and frequencies domain is presented in this chapter. System stability and controllability are discussed as well as issues related to the performance available in the motor system.
- **Controller Design:** and performance specifications are discussed in this chapter. The generalized plant and the mixed sensitivity setup is presented in relationship with H_∞ controller synthesis. The process of tuning a controller is described and the resulting controllers tested with regards to the performance specifications.
- **Real Time Programming:** includes an overview of the full system including the PC and AD/DA converts. The continuous controller is discretized, and a brief description of the program written for this project is offered.
- **Conclusion:** is an overview of positive test results and how well the objectives of the project are met.

CHAPTER 2

Analysis

Through the years many alternative approaches to the inverted pendulum problem have been taken. Some projects, including the one described in this thesis, deal with a pendulum standing on a cart that moves along a fixed axis and some projects are set up such that the pendulum is standing on a rotating disc [SP19]. The number of pendulum arms also varies between projects.
This project's primary control objective is to stabilize the pendulum in its vertical orientation and has reference tracking as a secondary objective. Projects that also deal with the problem of swinging up the pendulum from stable equilibrium (or any other initial condition) are quite impressive. These projects have different controller schemes for the separate objectives see [ZR01] and [NV13].
In this chapter alternative approaches to achieve the project objectives will be presented. No evaluation is made on if the alternative approaches are better or worse then the ones taken in this project, but rather to give a brief insight into how things have been done in the past.

2.1 Modelling alternatives

The mathematical modelling described in this thesis, was done using Newtonian mechanics. That is the interaction of torques and forces are used to describe the system. This approach is very convenient in some cases as a good approximation of simple systems can be acquired very quickly. However keeping track of vector directions, action and reaction of forces becomes increasingly harder as the complexity of the system grows.
As an alternative the Euler-Lagrange method (sometimes called Lagrange Hamilton Mechanics) utilizes the conservation of energy. To formulate the problem only the potential energy and the kinetic energy in the system needs to be defined, which in the case of the inverted double pendulum is fairly simple. How ever the math that follows might be a bit intimidating. In any case the two methods should deliver the same end result.

2.2 Controller design

There are of course many different approaches to the controller design. Conventional loop shaping is well suited for relatively simple problems but when it comes to stabilizing an unstable MIMO system it is probably not they way to go. Linear quadratic Regulator,

LQR, seems to be a popular choice for stabilizing the pendulum, with [ZR01] as an example. In terms of robustness LQR is perhaps not the best choice. It requires accurate plant model and thus is not robust to model uncertainties [SP05].
H_∞ optimisation method will be used for controller synthesis in this project, where the approach is taken to shape the closed loop sensitivity function S and controller sensitivity function KS in a so called mixed sensitivity setup. H_∞ optimization in the mixed sensitivity setup is also used in for the pendulum on a rotating disc in [SP19]. This optimisation method is used as well in the previous project of [Pou01] who takes a more complex signal based approach compared to the mixed sensitivity setup. The H_∞ optimisation method and the mixed sensitivity setup will be described in more detail later in this thesis.

2.3 Software implementation

One of the objectives of this project was to implement a discrete feedback controller. This would call for a real-time software that calculates the control signal and interprets measurement data while fulfilling strict requirements in execution time. It should establish connection with AD/DA converters to interact with the Test-Rig. Also the software should have some sort of a user interface, enabling the user operating the Test-Rig to interact with the system in real time. To simultaneously execute multiple objectives in software, time management is in general acquired through the use of program threads, task scheduling and with the use of semaphores.
For utilizing the computer appropriately for deterministic time response a real time operating system of some sort is needed to run this program. There are a number of real time operating systems on the market. To name a few Real-time Linux, FreeRTOS would have been good candidates for this project as they are free of use and operate on multiple platforms. In the previous project, Poulsen used OS9 running on a microcontroller[Pou01].
For this project Real Time Application Interface (RTAI) was the operating system running on the project computer. The reasons for choosing RTAI were both out of convenience and practicality. Since the author had some experience form real-time programming on a RTAI machine and such a machine was already set up and available for use in the laboratory this was the obvious choice.
For data acquisition on the real-time machine the *comedilib.h* library enabled interaction with Digital-to-Analog and Analog-to-Digital converters. Comedilib is a user-space library that provides a developer-friendly interface to Comedi devices [Sch]. Comedi stands for Control and Measurement Device Interface and is an open source application free of use.

2.4 Summary

From the discussion it is obvious that there are many ways to deal with the objectives of a project such as this one. The path taken in this particular project was mainly determined by the authors prior experience and what is considered to be most rewarding or useful in future projects.

CHAPTER 3

System Modeling

In this chapter the mathematical model of the system will be derived. This will be done in two steps, first for the pendulum sub-system and then for the motor sub-system. Finally these two sub-systems will be combined into a single nonlinear model describing the dynamics of the overall system.
For control purposes this chapter also describes how the linear state space model is acquired from the nonlinear model, which in Chapter 5 will be developed further into the generalized plant configuration.
Like stated in Chapter 1 the physical device was far from its optimal operating condition due to accumulated dirt, wear and tear. Wiring of the electronic circuit was also in very bad shape and parameters of the sensor circuit such as gains and offsets had to be adjusted. So in the following sections of this chapter (and Appendix C) the measures taken to get the device to operable conditions will be pointed out.

3.1 Analysis

There are many ways to go about getting a set of nonlinear differential equations that describe the system. Since the model used in this thesis is based on the previous work of [Pou01], who uses Newton's 2. and 3. law to describe the dynamics of the pendulum, that approach will be described in this chapter.
As an alternative the system was also modeled using a different approach, the Lagrange method. But since the model from [Pou01] had proved to give a good results both in simulation and for controller design, it was decided to continue using that model.
In Appendix A a model for the pendulum system is derived using the Lagrange method. The Lagrange method for the inverted double pendulum on a cart is also described in [ZR01]. In that paper the effect of friction is neglected and the interesting statement is made:

"Usually damping in under-actuated systems helps us to relax the conditions for stabilization. In this paper we do not consider internal frictions, so the DIP system with no internal damping represents the worst case for the implementation of various control strategies."[ZR01].

Here disturbances due to coulomb- and viscous friction are included in the model derivation, but eventually the choice is made to neglect the effect of viscous friction.

All parameters in the model are the same as used in [Pou01] with the exception of the gain of the of the speed controller embedded in the amplifier, since a new amplifier is used for this project. Numerical values can be found in Appendix B.

3.2 System description

A schematic of the pendulum system is shown in Figure 3.1. It consists of a cart, that slides on fixed rails along the x-axis. The lower arm of the pendulum is placed on top of the cart, and on top of the lower arm the upper arm is placed. The two arms are free to rotate around an axis perpendicular to the x-axis.
A motor is mounted at one end of the device (not shown in Figure 3.1). Trough a belt drive the rotary motion of the motor is transmitted to the linear motion of the cart. As stated before this system is an under-actuated system since it has only one actuator and three degrees of freedom (along the x-axis and rotation around the two joints of the arms). The actuator directly effects the position of the cart, but through the pendulum mechanics this linear motion translates to the dynamics of the pendulum.
As the arms of the pendulum divert from their vertical orientation the angles θ_1 and θ_2 increase in magnitude. This reduces the influence of the upward force F_{v1} from the cart on the lower arm, and the influence of F_{v2} from the lower arm on the upper arm. By placing the cart directly under the center of mass of the two arms, F_{v1} and F_{v2} cancel out the gravitational pull on the two arms $M_1 g$ and $M_2 g$ respectively. As a result the pendulum stands tall, stabilized in its unstable equilibrium.
The motor sub-system is constructed such that a servo amplifier with an embedded tacho-feedback speed controller, receives the control signal and is responsible for delivering the required energy to the DC-motor.

3.3 Pendulum model

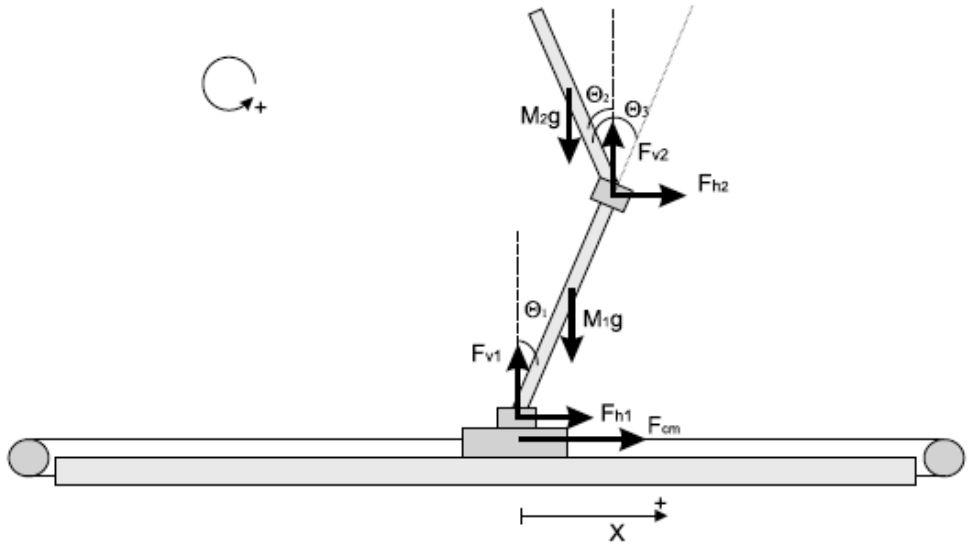

Figure 3.1: Principal diagram of the inverted double pendulum standing on the cart which is free to move along the x-axis. The two arrows pointing down represent the center of mass of the two arms, [Pou01].

Dynamics of the pendulum sub-system are fairly complex, so dynamical equations of the cart, lower arm and upper arm will be derived individually.

3.3.1 Cart

The force F_{cm} exerted on the cart, by the motor through the belt system, moves the cart along the x-axis. The force F_{h1} acting in the opposite direction is applied from the pendulum arms. Friction between the track and the cart is considered sufficiently low for it to be neglected in the model description.

$$M_0\ddot{x} = F_{cm} - F_{h1} \tag{3.1}$$

3.3.2 Lower arm

To describe the dynamics of the arms, the force vectors acting on them are projected into a horizontal and a vertical components, F_{hi} and F_{vi} respectively. The constant l_1 is the full length of the lower arm and l_{1cm} is the distance from the lower joint to the center of mass of the lower arm. M_1 is the mass of the lower arm.
Forces from the cart, the upper arm and earths gravity are exerted on the lower arm.

Horizontal:

$$M_1 \frac{d^2}{dt^2}[x + l_{1cm} sin\theta_1] = F_{h1} - F_{h2} \tag{3.2}$$

Vertical:

$$M_1 \frac{d^2}{dt^2}[l_{1cm} cos\theta_1] = F_{v1} - F_{v2} - M_1 g \tag{3.3}$$

The torque resulting from these forces on the lower joint, connecting the cart and lower arm, is found from Newtons 3. law.

Torque:

$$\begin{aligned} I_1 \ddot{\theta}_1 = &- F_{h1} l_{1cm} cos\theta_1 - F_{h2}(l_1 - l_{1cm}) cos\theta_1 + F_{v1} l_{1cm} sin\theta_1 \\ &+ F_{v2}(l_1 - l_{1cm}) sin\theta_1 - K_{v1}\dot{\theta}_1 - K_{d1} M_{d1} \end{aligned} \tag{3.4}$$

In Equation 3.4 the two last terms represent the friction in the lower joint. K_{d1} is a scale constant for the Coulomb friction and M_{d1} is the friction torque disturbance, not to be confused with the mass M_1, and takes the value 1 or -1 depending on direction of rotation. The viscous friction constant is eventually not included in the model so actually $K_{v1} = 0$, but the term is included in Equation 3.4 for the sake of completeness, or if the model is to be improved later on.

3.3.3 Upper arm

Forces from the lower arm and earths gravity are exerted on the upper arm. M_2 is the mass of upper arm and l_{2cm} is the distance from upper joint to the upper arm's center of mass.

Horizontal:

$$M_2 \frac{d^2}{dt^2}[x + l_1 sin\theta_1 + l_{2cm} sin\theta_2] = F_{h2} \tag{3.5}$$

Vertical:

$$M_2 \frac{d^2}{dt^2}[l_1 cos\theta_1 + l_{2cm} cos\theta_2] = F_{v2} - M_2 g \tag{3.6}$$

The torque resulting from these forces on the upper joint, connecting the lower arm to the upper arm, is found from Newtons 3. law.

Torque:

$$I_2 \ddot{\theta}_2 = - F_{h2} l_{2cm} cos\theta_2 + F_{v2} l_{2cm} sin\theta_2 - K_{v2}\dot{\theta}_2 - K_{d2} M_{d2} \tag{3.7}$$

Just as in Equation 3.4 the two last terms in Equation 3.7 represent the friction in the upper joint. K_{d2} is the Coulomb friction constant related to direction of rotation $M_{d2} \in \{-1, 1\}$, and again the viscous friction constant $K_{v2} = 0$.

3.4 Motor model

From the block diagram Figure 3.2 two differential equations are derived. One describing $\ddot{x}$, linear acceleration of the cart, and the other describing $\dot{i}$, the rate of change in current through the motor. The input U is the control signal and u is voltage at the motor terminal. The Torque Disturbance block has two terms. The first term describes the rotational friction inside the motor where K_{dm} is the friction constant and $M_{dm} \in \{-1, 1\}$ depending on direction of rotation. The second term is a function of F_{cm} which is influenced by the dynamics of the pendulum. F_{cm} appears in both the pendulum model and the motor model which is very convenient when combining the two systems in the overall model.

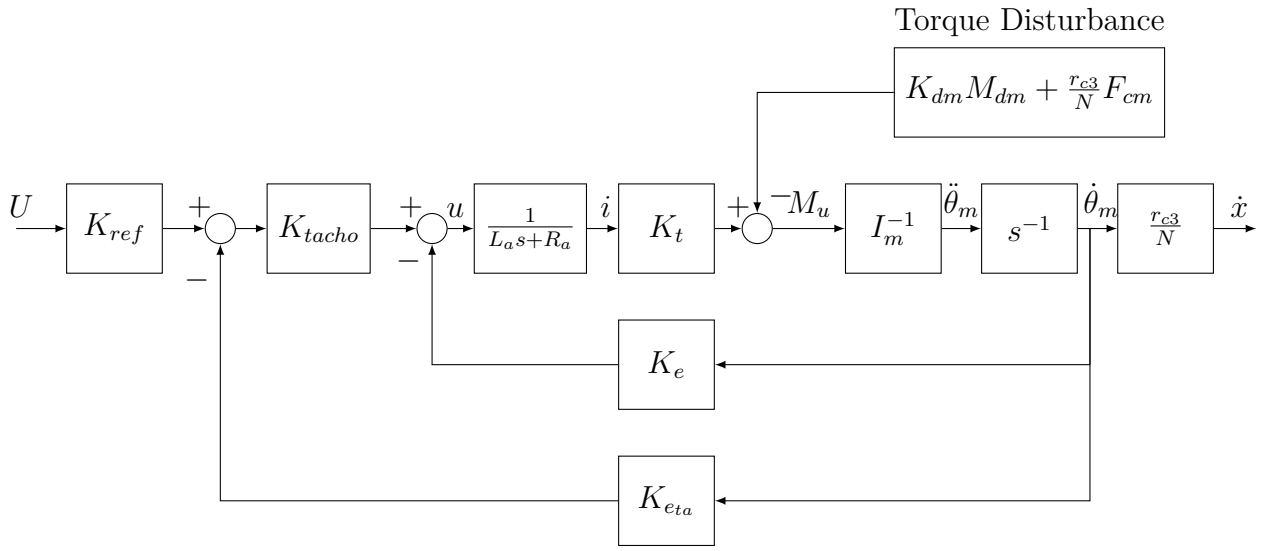

Figure 3.2: Block diagram of the motor with the tacho-feedback controller. K_{ref} and K_{taco} are adjustable parameters on the servo amplifier.

The voltage at the motor terminal can be expressed as,

$$u = K_{ref}K_{tacho}U - (K_e + K_{e_{ta}}K_{tacho})\dot{\theta}_m \tag{3.8}$$

Since the aim is to get an equation describing $\dot{i}$ another expression for motor voltage u, as a function of $\dot{i}$ and i, is needed. So Equation 3.9 is used to eliminate u.

$$u = L_a\dot{i} + R_a i \tag{3.9}$$

Combining and rearranging Equation 3.8-3.9 gives a differential equation describing the rate of change in the current $\dot{i}$.

$$\dot{i} = -\frac{(K_e + K_{e_{ta}} K_{tacho})}{La}\dot{\theta}_m - \frac{R_a}{L_a} i + \frac{K_{ref} K_{tacho}}{L_a} U \tag{3.10}$$

Eventually the pendulum system and the motor system are to be coupled together so a factor for converting angular dynamics of the motor shaft to the linear dynamics of the cart is needed. In Equation 3.11 N stands for the gear ratio and r_{c3} is the radius of the cog wheel.

$$x = \frac{r_{c3}}{N}\theta_m \tag{3.11}$$

If we rewrite Equation 3.10 using the relationship in Equation 3.11 we get a differential equation describing $\dot{i}$ as a function of the linear velocity of the cart $\dot{x}$, current through the motor i and the control signal U.

$$\dot{i} = -\frac{N}{r_{c3}}\frac{(K_e + K_{e_{ta}} K_{tacho})}{La}\dot{x} - \frac{R_a}{L_a} i + \frac{K_{ref} K_{tacho}}{L_a} U \tag{3.12}$$

Now taking a look at the motor torque M_u. As seen from Figure 3.2, the torque is a function of the current i and the Torque Disturbance block. By making use of $M_u = I_m \ddot{\theta}_m$ and Equation 3.11 an expression for $\ddot{x}$ is acquired and shown in Equation 3.15.

$$M_u = K_t i - (K_{dm} M_{dm} + \frac{r_{c3}}{N} F_{cm}) \tag{3.13}$$

$$I_m \ddot{\theta}_m = K_t i - (K_{dm} M_{dm} + \frac{r_{c3}}{N} F_{cm}) \tag{3.14}$$

$$\ddot{x} = \frac{r_{c3}}{N I_m} K_t i - \frac{r_{c3}}{N I_m} K_{dm} M_{dm} - \frac{r_{c3}^2}{N^2 I_m} F_{cm} \tag{3.15}$$

Equation 3.12 and 3.15 sufficiently describe the motor subsystem.

3.5 Full model

The simulator inherited from [Pou01], *DIPsys.mlx*, is set up in such a way that the motor part is a block model similar to the one shown in Figure 3.2 and the pendulum model is implemented algebraically in *nonlin_dip.m*. A very simplified version of the simulator is shown in Figure 3.3. In Appendix D a full description of the simulink model can be found along with the most important Matlab functions of the simulator.

For simulation purposes the nonlinear differential equations Equations 3.4, 3.7 and 3.15 sufficiently describe the system, but due to algebraic loops there is still work to be done before they are implemented in the Matlab function *nonlin_dip.m*.

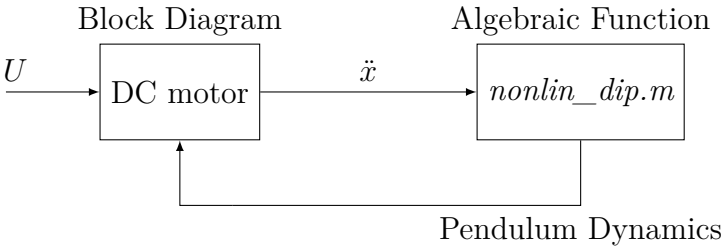

Figure 3.3: A simplified version of the nonlinear simulator implemented in Simulink. The Pendulum Dynamics affect the DC motor in the form of torque disturbance. The motor block is implemented as a block diagram but the pendulum block is implemented algebraically.

Equation 3.12, which describes $\dot{i}$, is not needed at this point since the dynamics of the motor are described by the DC-motor block diagram. However when the state space model is derived this equation will be of use.

Eliminating the algebraic loops in Equations 3.4 and 3.7, and coupling the two systems together via Equation 3.15 is a quite a messy process. After some trigonometric manipulation and inserting expressions for the vertical and horizontal forces $F_{v1,v2}$ and $F_{h1,h2}$, two equations are put forward.

$$\begin{aligned} &l_1 l_{2cm} M_2 cos(\theta_1 - \theta_2)\ddot{\theta}_1 + (l_{2cm}^2 M_2 + I_2)\ddot{\theta}_2 = \\ &- l_{2cm} M_2 cos\theta_2 \ddot{x} + l_1 l_{2cm} M_2 sin(\theta_1 - \theta_2)\dot{\theta}_1^2 \\ &- K_{v2}\dot{\theta}_2 + l_{2cm} M_2 sin\theta_2 g - K_{d2} M_{d2} \end{aligned} \tag{3.16}$$

$$\begin{aligned} &(l_{1cm}^2 M_1 + l_1^2 M_2 + I_1)\ddot{\theta}_1 + l_1 l_{2cm} M_2 cos(\theta_2 - \theta_1)\ddot{\theta}_2 = \\ &l_1 l_{2cm} M_2 sin(\theta_2 - \theta_1)\dot{\theta}_2^2 - (M_1 l_{1cm} + M_2 l_1) cos\theta_1 \ddot{x} \\ &+ (M_1 l_{1cm} + M_2 l_1) sin\theta_1 g - K_{v1}\dot{\theta}_1 - K_{d1} M_{d1} \end{aligned} \tag{3.17}$$

In order to simplify Equations 3.16 and 3.17, they may be written more conveniently in the following way, which in turn makes solving for $\ddot{\theta}_1$ and $\ddot{\theta}_2$ more manageable.

$$\begin{aligned} f_{11}\ddot{\theta}_1 + f_{12}\ddot{\theta}_2 &= f_{13} \\ f_{21}\ddot{\theta}_1 + f_{22}\ddot{\theta}_2 &= f_{23} \end{aligned}$$

$$
\begin{aligned}
f_{11} &= l_1 l_{2cm} M_2 cos(\theta_1 - \theta_2) \\
f_{12} &= (l_{2cm}^2 M_2 + I_2) \\
f_{13} &= -l_{2cm} M_2 cos\theta_2 \ddot{x} + l_1 l_{2cm} M_2 sin(\theta_1 - \theta_2)\dot{\theta}_1^2 - K_{v2}\dot{\theta}_2 + l_{2cm} M_2 sin\theta_2 g - K_{d2} M_{d2} \\
f_{21} &= (l_{1cm}^2 M_1 + l_1^2 M_2 + I_1) \\
f_{22} &= l_1 l_{2cm} M_2 cos(\theta_2 - \theta_1) \\
f_{23} &= l_1 l_{2cm} M_2 sin(\theta_2 - \theta_1)\dot{\theta}_2^2 - (M_1 l_{1cm} + M_2 l_1) cos\theta_1 \ddot{x} + (M_1 l_{1cm} + M_2 l_1) sin\theta_1 g \\
&\quad - K_{v1}\dot{\theta}_1 - K_{d1} M_{d1}
\end{aligned}
$$

$$\ddot{\theta}_1 = \frac{f_{13} f_{22} - f_{23} f_{12}}{f_{11} f_{22} - f_{21} f_{12}} \tag{3.18}$$

$$\ddot{\theta}_2 = \frac{f_{11} f_{23} - f_{21} f_{13}}{f_{11} f_{22} - f_{21} f_{12}} \tag{3.19}$$

Equations 3.18 and 3.19 fully describe the pendulum system and can be written as a function of variables as shown below.

$$\ddot{\theta}_1 = f(\theta_1, \dot{\theta}_1, \theta_2, \dot{\theta}_2, \ddot{x}, M_{d1}) \tag{3.20}$$

$$\ddot{\theta}_2 = f(\theta_1, \dot{\theta}_1, \theta_2, \dot{\theta}_2, \ddot{x}, M_{d2}) \tag{3.21}$$

The final step here is to couple the motor system and the pendulum system together through F_{cm}. Starting with the following expression derived from equations in Chapter 3.4.

$$
\begin{aligned}
F_{cm} &= (M_0 + M_1 + M_2)\ddot{x} - (M_1 l_{1cm} sin\theta_1 + M_2 l_1 sin\theta_1)\dot{\theta}_1^2 - M_2 l_{2cm} sin\theta_2 \dot{\theta}_2^2 \\
&\quad + (M_1 l_{1cm} cos\theta_1 + M_2 l_1 cos\theta_1)\ddot{\theta}_2
\end{aligned} \tag{3.22}
$$

Inserting Equation 3.22 into Equation 3.15, $\ddot{x}$ may be written as,

$$
\begin{aligned}
\ddot{x} &= \frac{K_t}{C_x} i - K_{vm} \frac{N}{r_{c3} C_x} \dot{x} - \frac{K_{dm}}{C_x} M_{dm} + \frac{r_{c3}}{NCx} (M_1 l_{1cm} sin\theta_1 + M_2 l_1 sin\theta_1)\dot{\theta}_1^2 \\
&\quad + \frac{r_{c3}}{NC_x} M_2 l_{2cm} sin\theta_2 \dot{\theta}_2^2 - \frac{r_{c3}}{NC_x} (M_1 l_{1cm} cos\theta_1 + M2l1 cos\theta_1)\ddot{\theta}_1 \\
&\quad - \frac{r_{c3}}{N} M_2 l_{2cm} cos\theta_2 \ddot{\theta}_2
\end{aligned} \tag{3.23}
$$

where

$$C_x = I_m \frac{N}{r_{c3}} + \frac{r_{c3}}{N}(M_0 + M_1 + M_2) \tag{3.24}$$

Now by inserting Equations 3.20 and 3.21 into Equation 3.23 three nonlinear differential equations have been derived without algebraic loops and are ready to be implemented in *nonlin_dip.m* for simulation.

$$\ddot{\theta}_1 = f(\theta_1, \dot{\theta}_1, \theta_2, \dot{\theta}_2, \dot{x}, i, M_{d1}) \tag{3.25}$$
$$\ddot{\theta}_2 = f(\theta_1, \dot{\theta}_1, \theta_2, \dot{\theta}_2, \dot{x}, i, M_{d2}) \tag{3.26}$$
$$\ddot{x} = f(\theta_1, \dot{\theta}_1, \theta_2, \dot{\theta}_2, M_{d1}, M_{d2}, \dot{x}, i, M_{dm}) \tag{3.27}$$

3.6 State space model

Like for the non-linear model, the state space model will be derived separately for the two subsystems and then eventually combined into one.
Beginning with the motor system, the first step is to define the state vector x_m, disturbance input vector ω_m, control input vector u_m and the output vector v_m. Later on $\ddot{x}$ will be defined as an input to the pendulum model, so here it is chosen to be the output of the motor model. Note that the disturbance input vector includes measurement noise n_x entering the system through a scaling constant K_{nx}.

$$x_m = \begin{bmatrix} x \\ \dot{x} \\ i \end{bmatrix} \quad \omega_m = \begin{bmatrix} M_{dm} \\ n_x \end{bmatrix} \quad u_m = [U] \quad v_m = [\ddot{x}] \tag{3.28}$$

To set up the state space model, equations that describe $\ddot{x}$ and $\dot{i}$ are needed. Equations 3.12 and 3.15 do exactly that and are shown below. Note that the force F_{cm} depends on the dynamics of the pendulum which is useful when the two systems are coupled together.

$$\dot{i} = -\frac{N}{r_{c3}} \frac{(K_e + K_{e_{ta}} K_{tacho})}{La} \dot{x} - \frac{R_a}{L_a} i + \frac{K_{ref} K_{tacho}}{L_a} U$$
$$\ddot{x} = \frac{r_{c3}}{N I_m} K_t i - \frac{r_{c3}}{N I_m} K_{dm} M_{dm} - \frac{r_{c3}^2}{N^2 I_m} F_{cm}$$

$$\dot{x}_m = A_m x_m + B_{1m} \omega_m + B_{2m} u_m + B_p F_{cm} \tag{3.29}$$
$$\dot{v}_m = C_m x_m + D_{1m} \omega_m + D_{2m} u_m + D_p F_{cm}$$

$$
\begin{aligned}
A_m &= \begin{bmatrix} 0 & 1 & 0 \\ 0 & 0 & K_t \frac{r_{c3}}{NI_m} \\ 0 & -(K_e + K_{e_{ta}} K_{tacho}) \frac{N}{L_a r_{c3}} & -\frac{R_a}{L_a} \end{bmatrix} \\
B_{1m} &= \begin{bmatrix} 0 & 0 \\ -K_{dm} \frac{r_{c3}}{I_m N} & 0 \\ 0 & 0 \end{bmatrix} \\
B_{2m} &= \begin{bmatrix} 0 \\ 0 \\ \frac{K_{ref} K_{tacho}}{L_a} \end{bmatrix} \\
B_p &= \begin{bmatrix} 0 \\ -\frac{r_{c3}^2}{N^2 I_m} \\ 0 \end{bmatrix} \\
C_m &= \begin{bmatrix} 0 & 0 & K_t \frac{r_{c3}}{NI_m} \end{bmatrix} \\
D_{1m} &= \begin{bmatrix} -K_{dm} \frac{r_{c3}}{NI_m} & K_{nx} \end{bmatrix} \\
D_{2m} &= [0] \\
D_p &= \begin{bmatrix} -\frac{r_{c3}^2}{N^2 I_m} \end{bmatrix}
\end{aligned}
\tag{3.30}
$$

The state vector, input and output vectors for the pendulum model are defined below. Just as for the motor model here is were measurement noise is introduced to the model. n_1 and n_3 are noise signal expected on the two angle measurement

$$
x_p = \begin{bmatrix} \theta_1 \\ \dot{\theta}_1 \\ \theta_2 \\ \dot{\theta}_2 \end{bmatrix} \quad \omega_p = \begin{bmatrix} M_{d1} \\ M_{d2} \\ n_1 \\ n_3 \end{bmatrix} \quad u_p = [\ddot{x}] \quad v_p = \begin{bmatrix} \dot{\theta}_1 \\ \dot{\theta}_3 \end{bmatrix} \tag{3.31}
$$

Unlike the dynamic equations of the motor, Equations 3.20 and 3.21 describing the pendulum are nonlinear and need to be linearized around the operating conditions. The effect of viscous friction is neglected which eliminates terms related to angular velocity $\dot{\theta}_1$ and $\dot{\theta}_2$. Conveniently the control objective is to minimize the angular position, θ_1 and θ_2, so the trigonometric functions of the two equations may be linearized using the small angle approximation.

$$
\begin{aligned}
cos\theta &\approx 1 \quad for\ small\ \theta \\
sin\theta &\approx \theta \quad for\ small\ \theta
\end{aligned}
$$

The resulting lineraized equations set up in the state space form,

$$\begin{aligned} \dot{x}_p &= A_p x_p + B_{1p}\omega_p + B_{2p}u_p \\ \dot{v}_p &= C_p x_p + D_{1p}\omega_p + D_{2p}u_p \end{aligned} \tag{3.32}$$

$$\begin{aligned}
A_p &= \begin{bmatrix} 0 & 1 & 0 & 0 \\ \frac{(M_1 l_{1cm} + M2_{l1})(I_2 + M_2 l_{2cm}^2)}{C_{den}} g & 0 & -\frac{M_2^2 l_{2cm}^2 l_1}{C_{den}} g & 0 \\ 0 & 0 & 0 & 1 \\ -\frac{M_2 l_1 l_{2cm}(M_1 l_{1cm} + M_2 l_1)}{C_{den}} g & 0 & \frac{M_2 l_{2cm}(I_1 + M_1 l_{1cm}^2 + M_2 l_1^2)}{C_{den}} g & 0 \end{bmatrix} \\
B_{1p} &= \begin{bmatrix} 0 & 0 & 0 & 0 \\ \frac{K_{d1}(M_2 l_{2cm}^2 + I_2)}{C_{den}} & -\frac{K_{d2} M_2 l_1 l_{2cm}}{C_{den}} & 0 & 0 \\ 0 & 0 & 0 & 0 \\ -\frac{K_{d1} M_2 l_{2cm} l_1}{c_{den}} & \frac{K_{d2}(M_1 l_{1cm}^2) + M_2 l_1^2 + I_2}{C_{den}} & 0 & 0 \end{bmatrix} \\
B_{2p} &= \begin{bmatrix} 0 \\ \frac{M_2 l_{2cm}^2 l_1 - (M_1 l_{1cm} + M_2 l_1)(M_2 l_{2cm}^2 + I_2)}{C_{den}} \\ 0 \\ -\frac{M_2 l_{2cm}(M_1 l_{1cm}^2 + M_2 l_1^2 + I_1) + M_2 l_1 l_{2cm}(M_1 l_{1cm} + M_2 l_1)}{C_{den}} \end{bmatrix} \\
C_p &= \begin{bmatrix} 1 & 0 & 0 & 0 \\ -1 & 0 & 1 & 0 \end{bmatrix} \\
D_{1p} &= \begin{bmatrix} 0 & 0 & K_{n_1} & 0 \\ 0 & 0 & 0 & K_{n_3} \end{bmatrix} \\
D_{2p} &= \begin{bmatrix} 0 \\ 0 \end{bmatrix}
\end{aligned} \tag{3.33}$$

where the common denominator of A_p, B_{1p} and B_{2p} is shown below.

$$C_{den} = (M_1 l_{1cm}^2 + M_2 l_1^2 + I_1)(M_2 l_{2cm}^2 + I_2) - (M_2 l_1 l_{2cm})^2$$

To combine the two sub-systems into a single state space model the state vector x for this full model, as well as disturbance input vector ω, control input vector u and output vector v are defined. Note that here the reference input for the cart position r_x is introduced. It follows, as one would expect, that one of the outputs is $e_x = r_x - x$, the cart position error along with the two angles θ_1 and θ_3. Eventually the objective is to minimize θ_2 rather then θ_3, but for now this how the output vector is defined.

$$x = \begin{bmatrix} \theta_1 \\ \dot{\theta}_1 \\ \theta_2 \\ \dot{\theta}_2 \\ x \\ \dot{x} \\ i \end{bmatrix} \quad \omega = \begin{bmatrix} r_x \\ M_{d1} \\ M_{d2} \\ n_1 \\ n_3 \\ M_{dm} \\ n_x \end{bmatrix} \quad u = [U] \quad v = \begin{bmatrix} e_x \\ \theta_1 \\ \theta_3 \end{bmatrix} \tag{3.34}$$

Linearizing Equation 3.23 gives the following equation for $\ddot{x}$, where C_x is as defined in Equation 3.24 and $\dot{x}_p = \begin{bmatrix} \dot{\theta}_1 & \ddot{\theta}_2 & \dot{\theta}_2 & \ddot{\theta}_2 \end{bmatrix}$ the derivative of the state vector of the pendulum model.

$$\begin{aligned} \ddot{x} &= \frac{K_t}{C_x} i - \frac{K_{dm}}{C_x} M_{dm} - \frac{r_{c3}}{NCx} \begin{bmatrix} 0 & M_1 l_{1cm} + M_2 l_1 & 0 & M_2 l_{2cm} \end{bmatrix} \dot{x}_p \\ &= \frac{K_t}{C_x} i - \frac{K_{dm}}{C_x} M_{dm} + D_p \dot{x} \end{aligned} \tag{3.35}$$

For some reason Poulsen has two definitions for C_x that appear different, but mathematically they are the same (one definition in his thesis and another definition in Appendix B of his thesis)[Pou01]. This is only to cause confusion, so in this thesis C_x is only defined once and is the same as used for Matlab implementation. It has been verified that this does not affect numerical results, even though appearance might differ. Equation 3.29 is now rewritten such that it includes the dynamics of the pendulum $\dot{x}_p$.

$$\begin{aligned} \dot{x}_m &= A_m x_m + B_{1m} \omega_m + B_{2m} u_m + B_p \dot{x}_p \\ \dot{v}_m &= C_m x_m + D_{1m} \omega_m + D_{2m} u_m + D_p \dot{x}_p \end{aligned} \tag{3.36}$$

Where D_p is a shown in Equation 3.35 and to construct B_p, $\bar{0}$ are appropriately sized vectors full of zeros.

$$B_p = \begin{bmatrix} \bar{0} \\ D_p \\ \bar{0} \end{bmatrix} = \begin{bmatrix} 0 & 0 & 0 & 0 \\ 0 & -\frac{r_{c3}}{NCx}(M_1 l_{1cm} + M_2 l_1) & 0 & -\frac{r_{c3}}{NCx}(M_2 l_{2cm}) \\ 0 & 0 & 0 & 0 \end{bmatrix}$$

Now, inserting Equation 3.32 eliminating $\dot{x}_p$

$$\begin{aligned} \dot{x}_m &= A_m x_m + B_{1m} \omega_m + B_{2m} u_m + B_p (A_p x_p + B_{1p} \omega_p + B_{2p} u_p) \\ v_m &= C_m x_m + D_{1m} \omega_m + D_{2m} u_m + D_p (A_p x_p + B_{1p} \omega_p + B_{2p} u_p) \end{aligned} \tag{3.37}$$

Since $u_p = v_m$ the output equation for the motor system is rewritten, and v_m terms collected.

$$\begin{aligned} v_m &= C_m x_m + D_{1m}\omega_m + D_{2m}u_m + D_p A_p x_p + D_p B_{1p}\omega_p + D_p B_{2p} v_m \\ &= C_m(I - DpB_{2p})^{-1}x_m + D_{1m}(I - DpB_{2p})^{-1}\omega_m + D_{2m}(I - DpB_{2p})^{-1}u_m \\ &\quad + D_p A_p(I - DpB_{2p})^{-1}x_p + D_p B_{1p}(I - DpB_{2p})^{-1}\omega_p \end{aligned} \tag{3.38}$$

Combining the two systems, with this new expression for v_m

$$\begin{aligned} \dot{x}_p &= A_p x_p + B_{1p}\omega_p + B_{2p} v_m \\ &= A_p x_p + B_{1p}\omega_p + B_{2p}\Big[C_m(I - DpB_{2p})^{-1}x_m + D_{1m}(I - DpB_{2p})^{-1}\omega_m \\ &\quad D_{2m}(I - DpB_{2p})^{-1}u_m + D_p A_p(I - DpB_{2p})^{-1}x_p + D_p B_{1p}(I - DpB_{2p})^{-1}\omega_p\Big] \end{aligned}$$

Collecting terms with some matrix algebra gives

$$\begin{aligned} \dot{x}_p &= (A_p + B_{2p}D_p A_p)(I - D_p B_{2p})^{-1}x_p + (B_{2p}C_m)(I - D_p B_{2p})^{-1}x_m \\ &\quad + (B_{1p} + B_{2p}D_p A_p)(I - D_p + B_{2p})^{-1}\omega_p + (B_{2p}D_{1m})(I - D_p + B_{2p})^{-1}\omega_m \\ &\quad + (B_{2p}D_{2m})(I - D_p + B_{2p})^{-1}u_m \end{aligned} \tag{3.39}$$

$$v_p = C_p x_p + D_{1p}\omega_p \tag{3.40}$$

Similarly, terms are collected in Equation 3.37 and the motor system is rewritten.

$$\begin{aligned} \dot{x}_m &= (B_{2p}C_m)(I - D_p B_{2p})^{-1}x_p + (A_m + (B_p B_{2p}C_m)(I - D_p B_{2p})^{-1})x_m \\ &\quad + (B_p(B_{1p} + B_{2p}D_p B_{1p})(I - D_p B_{2p})^{-1})\omega_p + (B_{1m} + B_p B_{2p}D_{1m}(I - D_p B_{2p})^{-1})\omega_m \\ &\quad + (B_{2m} + B_p B_{2p}D_{2m}(I - D_p B_{2p})^{-1})u_m \end{aligned} \tag{3.41}$$

With Equations 3.38-3.41 a full state space model can be put forward with the desired state vector and input and output vectors seen in Equation 3.42.

$$\begin{aligned}
\begin{bmatrix} \dot{x}_p \\ x_m \end{bmatrix} &= A \begin{bmatrix} x_p \\ x_m \end{bmatrix} + B_1 \begin{bmatrix} \omega_p \\ \omega_m \end{bmatrix} + B_2 u_m \\
\begin{bmatrix} v_p \\ v_m \end{bmatrix} &= C \begin{bmatrix} x_p \\ x_m \end{bmatrix} + D_1 \begin{bmatrix} \omega_p \\ \omega_m \end{bmatrix} + D_2 u_m \\
&\downarrow \\
\dot{x} &= Ax + B_1\omega + B_2 u \\
v &= Cx + D_1\omega + D_2 u
\end{aligned} \tag{3.42}$$

A complete description of the vectors of the state space model are shown in Equation 3.43.

$$x = \begin{bmatrix} \theta_1 \\ \dot{\theta}_1 \\ \theta_2 \\ \dot{\theta}_2 \\ x \\ \dot{x} \\ i \end{bmatrix} \quad \omega = \begin{bmatrix} r_x \\ M_{d1} \\ M_{d2} \\ n_1 \\ n_3 \\ M_{dm} \\ n_x \end{bmatrix} \quad u = [U] \quad v = \begin{bmatrix} e_x \\ \theta_1 \\ \theta_3 \end{bmatrix} \tag{3.43}$$

The matrices of the state equation can are defined below. The $\bar{0}$ indices in B_1 are appropriately sized matrices full of zeros.

$$A = \begin{bmatrix} (A_p + B_{2p}D_pA_p)(I - D_pB_{2p})^{-1} & (B_{2p}C_m)(I - D_pB_{2p})^{-1} \\ B_p(A_p + B_{2p}D_p)(I - D_pB_{2p})^{-1} & A_m + (B_pB_{2p}C_m)(I - D_pB_{2p})^{-1} \end{bmatrix} \tag{3.44}$$

$$B_1 = \begin{bmatrix} \bar{0} & (B_{1p} + B_{2p}D_pB_{1p})(I - D_pB_{2p})^{-1} & (B_{2p}D_{1m})(I - D_pB_{2p})^{-1} \\ \bar{0} & B_p(B_{1p} + B_{2p}D_pB_{1p})(I - D_pB_{2p})^{-1} & B_{1m} + B_p(B_{2p}D_{1m})(I - D_pB_{2p})^{-1} \end{bmatrix} \tag{3.45}$$

$$B_2 = \begin{bmatrix} B_{2p}D_{2m}(I - D_pB_{2p})^{-1} \\ B_{2m} + B_pB_{2p}D_{2m}(I - D_pB_{2p})^{-1} \end{bmatrix} \tag{3.46}$$

Finally, to conclude this section, the matrices of the output equation are defined below.

$$C = \begin{bmatrix} 0 & 0 & 0 & 0 & -1 & 0 & 0 \\ 1 & 0 & 0 & 0 & 0 & 0 & 0 \\ -1 & 0 & 1 & 0 & 0 & 0 & 0 \end{bmatrix} \tag{3.47}$$

$$D_1 = \begin{bmatrix} 1 & 0 & 0 & 0 & 0 & 0 & -K_{n_x} \\ 0 & 0 & 0 & K_{n_1} & 0 & 0 & 0 \\ 0 & 0 & 0 & 0 & K_{n_3} & 0 & 0 \end{bmatrix} \tag{3.48}$$

$$D_2 = \begin{bmatrix} 0 \\ 0 \\ 0 \end{bmatrix} \tag{3.49}$$

3.7 Verification

The mathematical modeling of the system is far from straight forward. As stated earlier, the method described in this chapter is based on the work of [Pou01]. Reviewing his work there were two instances where the equations described in his thesis did not match the equations implemented in his Matlab code used for controller design and simulations. Below these errors are listed and the equation numbers point to equations of this thesis that correspond to the erroneous equations in [Pou01].

- In Equation 3.30 K_{n_x} was missing from the D_{1m} matrix.
- In Equation 3.33 g was missing from both indices in the second row of the A_p matrix.
- Indecies related to x_p and ω_p in matrices A and B_1, Equation 3.44-3.45 were simply wrong

In this thesis all equations above are in agreement with the equations in the Matlab file *model.m* from the previous project, and have been verified analytically.

3.7.1 Flaw in the pendulum model

Like already stated Appendix A offers a different approach to the modeling of the system, using the Lagrange method. The Lagrange method deals with the problem by utilizing the preservation of energy in the system, rather then the interaction of forces. Ideally both methods should yield the same results, and this is true in all aspects besides one. It turns out that the two models differ when it comes to the input matrix B_{2p}, which describes how the cart acceleration affects the dynamics of the pendulum.
In the following comparison G is the state space model derived above, and G_{alt} is the

state space model derived with the Lagrange method. As seen in Equations 3.50-3.51 the numerical values in both B_{2p} matrices are the same but with opposite signs.

$$\dot{x}_p = A_p x_p + B_{1p}\omega_p + B_{2p}\ddot{x}$$

$$G: \quad B_{2p} = \begin{bmatrix} 0 \\ -1.9842 \\ 0 \\ 0.1881 \end{bmatrix} \tag{3.50}$$

$$G_{alt}: \quad B_{2p} = \begin{bmatrix} 0 \\ 1.9842 \\ 0 \\ -0.1881 \end{bmatrix} \tag{3.51}$$

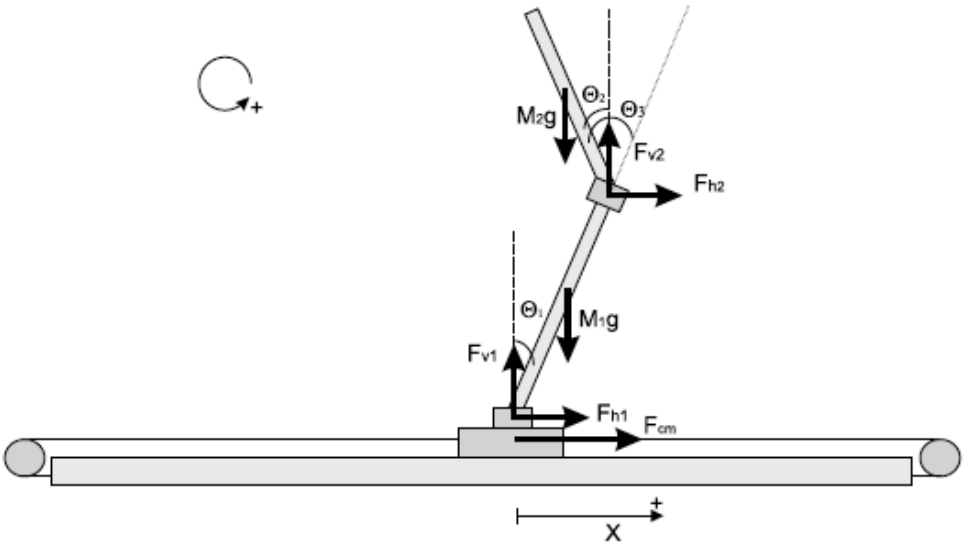

Figure 3.4: The frame of reference defined does not match the mathematical model, [Pou01].

The frame of reference in Figure 3.4, is defined such that a positive movement along the x-axis is from left to right, and positive angular movement is counter-clockwise. In reality, if arms are initialized fully vertical, a positive linear acceleration of $\ddot{x}$ results in a positive $\ddot{\theta}_1$ and a negative $\ddot{\theta}_2$.
This is exactly the relationship is described in G_{alt} but not in G.
To demonstrate this, rather the diving into the complex math, two simulations are done on both state space models.

- System initialized such that $\theta_1 = 0.2$ causing gravity to pull down the two arms of the pendulum. Initial conditions $[x,\ \theta_1,\ \theta_2] = [0,\ 0.2,\ 0]$.

- System initialized with both arms fully vertical and a step in the control voltage is applied. Initial conditions $[x,\ \theta_1,\ \theta_2] = [0,\ 0,\ 0]$

Figure 3.5 shows how the systems respond when only excited by gravity and Figure 3.6 shows how the two systems respond to a step input applied to the motor with both arms oriented vertically.

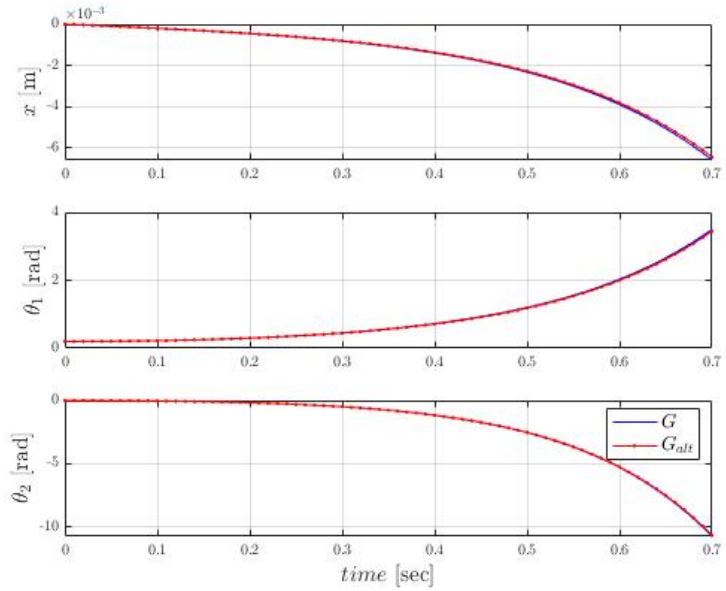

Figure 3.5: The two systems have very similar dynamics when only excited by gravity. The counter-clockwise fall of the lower arm, seems to drag the cart to the left.

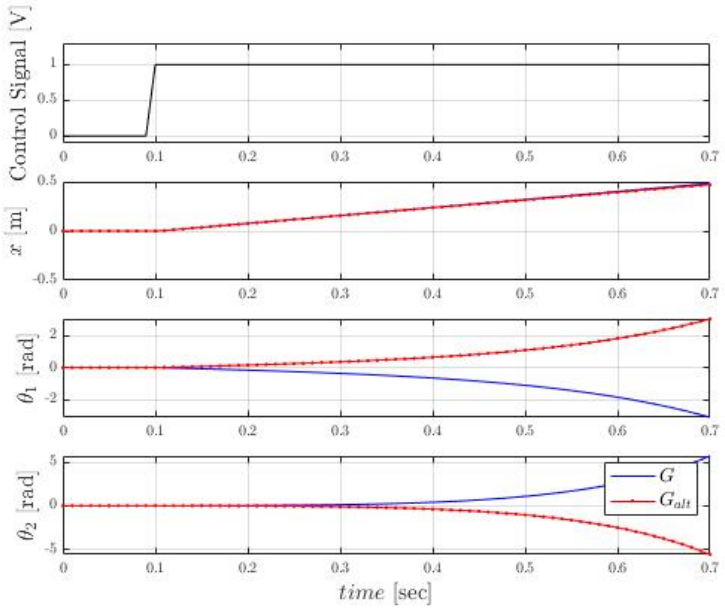

Figure 3.6: Step input is applied to the motor. Note that a positive acceleration of the cart should result in θ_1 to increase and θ_2 to decrease. G_{alt} shows this behaviour but not G.

Figure 3.6 shows that the two models don't agree on direction of rotation, even tough they are derived from the same principal diagram, and therefore have the same frame of reference. The blue line shows that as x increases θ_1 decreases (rotates clockwise). On the other hand G_{alt}, from the Lagrange method, more realistically represents the dynamics of the system, where positive acceleration in x results in a counterclockwise movement in θ_1.

The state space model G is derived from the same equations used for the nonlinear simulator. So one suspects that the flaw might also be apparent in the simulator. To check this a similar experiment is done as described above, that is comparing the Test-Rig to the simulator when as step input is applied to the motor. Figure 3.7 shows that the simulator behaves as the state space model G in Figure 3.6. The response of the Test-Rig is how ever better described by G_{alt}.

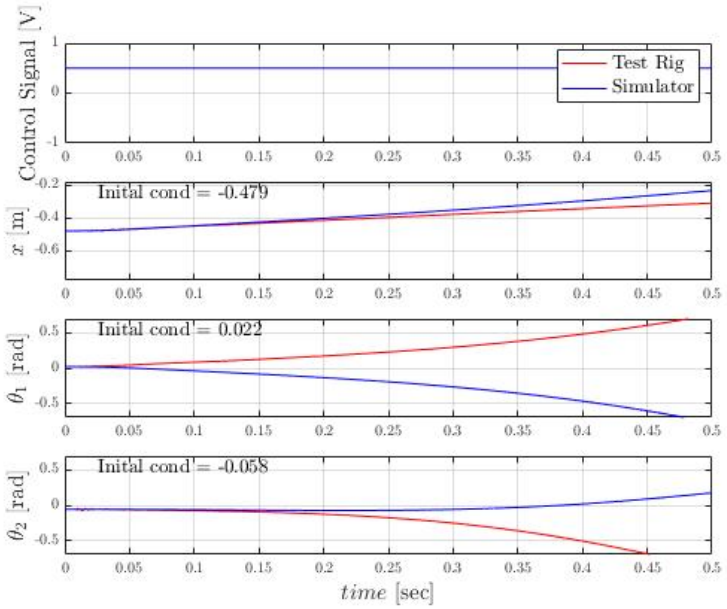

Figure 3.7: The nonlinear simulator shows similar dynamics as G, whereas G_{alt} behaves like the Test-Rig.

In a sense both models are correct as they both sufficiently describe the dynamics of the system. However, when it comes to implementing a controller on the Test-Rig, care should be taken to ensure that the frame of reference of the Test-Rig is in agreement with the mathematical model.

3.7.2 Motor and Amplifier

The biggest difference between this project and the one done by Poulsen is that a different amplifier is used to drive the motor [Pou01]. In both projects the amplifier has a tacho feedback speed controller. Naturally, care had to be taken to ensure that the new amplifier had similar gain values as the gains from the old system. So K_{ref} and K_{tacho} had to be tuned such that the model matched the Test-Rig with this new amplifier.
Tuning the new amplifier was done by applying 0V to the amplifier input, indicating zero velocity. First an internal offset adjustment was tuned such that the motor showed no angular movement, equivalently no linear movement of the cart. Then K_{tacho} was adjusted such that a fair amount of external force on the cart did not result in the cart moving. Meaning that the embedded speed controller was working hard in maintaining the zero velocity reference input. Finally K_{ref} was tuned by inspection of the the step response of the motor system seen in Figure 3.8, ensuring the model and motor subsystem of the Test-Rig had similar responses.
The amplifier used in this project also had current limiter which had not been included in the simulator from [Pou01] and had to be added as a saturation block.

Comparison between the Test-Rig and the simulator, with new gain values and a ±8A current limiter, can be seen in Figure 3.8. The motor part of the simulator matches the corresponding part of the Test-Rig quite well.

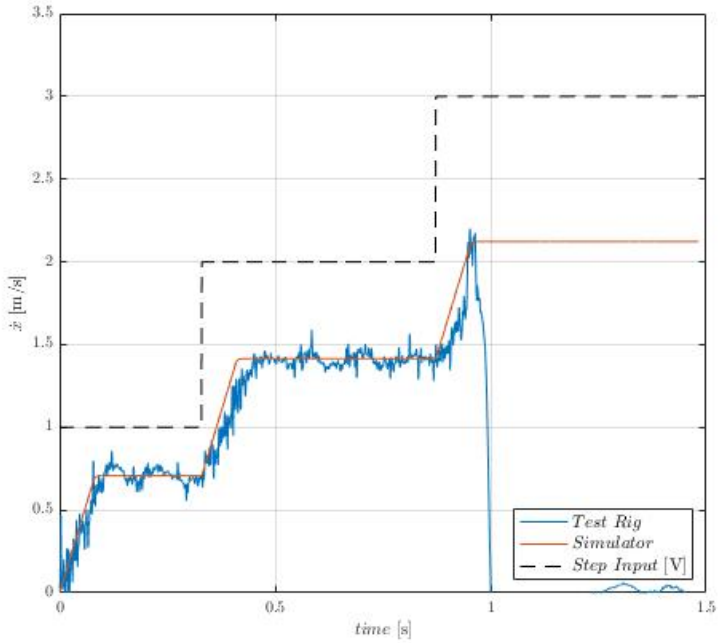

Figure 3.8: Three step control input applied to the motor in simulation and on the Test-Rig. Note that the sudden drop in Test-Rig velocity is due to the cart reaching the end of the track.

3.8 Summary

The inverted double pendulum system is rather complex, and modeling this system is far from an easy task. In the derivation above the interactions of torques and forces has been used to acquire differential equations that describe the system. As it turns out it seems that the resulting model does not agree with the real world, or at least not to the frame of reference defined in Figure 3.1, as explained in Chapter 3.8.1. The origin of this error has not been found, but it appears in the matrix B_{2p} and thus in all indices of A, B_1 and B_2 in Equations 3.44-3.46
Even though this potential error in modelling can be easily compensated for by inverting the signs on the angle measurements, such that positive angular movement becomes clockwise, it is really hard to evaluate whether this error affects the pendulum model in other and more subtle ways. This has caused a lot of confusion, specially with regard to the implementation of the discrete controller presented in Chapter 6. and ideally this flaw should have been investigated further on the Test-Rig.

For motor and amplifier part of the systems, Figure 3.8 shows that simulator and the Test-Rig are very similar. So it is concluded that in terms of the motor sub-system the simulator is a good representation of the Test-Rig. The bad news is that the current limiting feature of the new amplifier puts boundaries on the the performance available from the system's only actuator. This will be investigated further in next chapter.

CHAPTER 4

System Analysis

In this chapter information is about the system is gathered, both in frequency domain and time domain. This information will be useful when it comes to design a controller. Since analysis is done primarily on the mathematical model, rather then the real system, all flaws in the model will be carried through into analysis. Off course there is no such thing as a perfect model. There are unknown dynamics within the system, parameters of the model such as friction do change over time and due to measurement imperfections measured values most likely deviate from their true value. Finally the state space model used for analysis is a linear approximation of the non-linear approximation of the real system.
The subject of Chapter 3.8.1, where the flaw in the model is addressed, might as well be included in this chapter. In that chapter it is concluded that, besides the model not being according to the frame of reference originally defined, the model is a fairly good approximation of the real system.

4.1 Time domain analysis

Like mentioned in Chapter 3, the amplifier in the Test-Rig has a current limiter. So a current limiter was added to the motor sub-system of the simulator. Figure 3.8 shows that when the simulator includes a ± 8A limiter, it is a good representation of the response of the real system. Figure 4.1 shows a comparison of the cart velocity for the system with an ideal amplifier, having no current limiter, and the system with a current limiting amplifier.

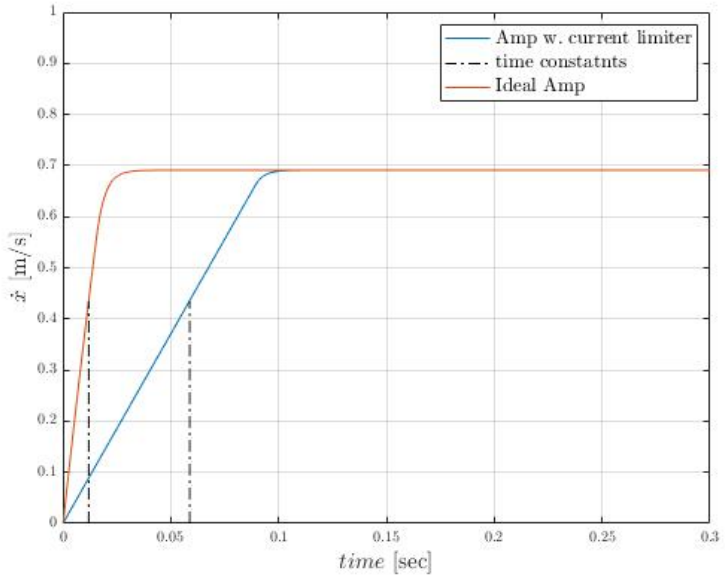

Figure 4.1: Motor system response to a 1V step input. The current limiting feature of the motor amplifier slows down the response of the system. The vertical dashed lines indicate the time constant of the two systems.

This current limiting feature of the amplifier significantly slows down the response of the motor. Comparison of the time constants of the two systems shows that the system with ideal amplification is about 6 times faster then system with the amplifier in the Test-Rig, limiting the performance available in the actuator. Figure 4.2 shows the amplitude of the current flowing through the motor in the two systems. Of course the current limiter serves the purpose of protecting the motor from getting exposed to high current amplitudes, that can damage the actuator.
According to the motor data sheet the stall torque of the motor is $M_H = 510\text{mNm}$ and the current constant is $k_i = 0.047\text{A/mNm}$, multiplying these constants gives $M_H k_i = 23.97\text{A}$. This is an indication of how much current the motor should be able to withstand, at least for a short period of time. So limiting the current spikes at $i \approx \pm 24\text{A}$ would be more reasonable.

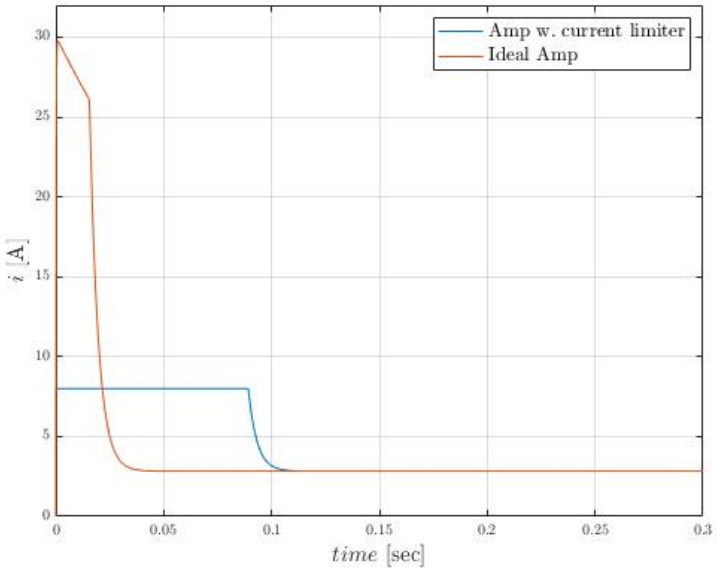

Figure 4.2: Current flowing through the motor in the case of the ideal amplifier and in the case of the amplifier with a current limiter. Initial moments of the current in the ideal amp show a linear downward slope, this is due to the tacho feedback loop of the amplifier only being able to handle $\pm 10V$.

4.2 Frequency domain analysis

Now taking a look at system dynamics in frequency domain. Like already stated the uncontrolled system is unstable. Intuition indicates that if the pendulum is released from a vertical orientation the pendulum arms will fall to the sides. In analysis of control systems, stability is achieved when all poles of a transfer function lie in the left-half of the s-plane, or equivalently, that all eigenvalues of the system matrix A are negative [DB17].

$$\lambda(A) = \left\{ \begin{array}{c} 0 \\ -7335.6 \\ -336.8 \\ 6.4 \\ 4.1 \\ -4.1 \\ -6.4 \end{array} \right\} \tag{4.1}$$

The eigenvalues, listed in Equation 4.1, consist of two very high negative values, belonging to the motor sub-system, two pole pairs that belong to the pendulum sub system and a zero. The positive eigenvalues of these pairs show that the system is unstable as expected.

Figure 4.3 shows how the control signal u affects all three outputs of the system, cart position and angular position of the joints. No control is applied to the system besides the tacho-feedback speed control embedded in the motor amplifier. This speed controller allows tight control of the cart position x at low frequencies.
The frequency response of the angles θ_1, θ_2 and θ_3 have peaks in the range 5-10 rad/s. It should be kept in mind that θ_2 and θ_3 are actually rotating around the same joint. The difference being that θ_3 is measured with respect to θ_1 but θ_2 measured with respect to vertical. Recall that from Figure 3.4 that,

$$\theta_2 = \theta_1 + \theta_3$$

so as depicted in Figure 4.3 at low frequencies when the magnitude of θ_3 is low, θ_2 closely follows θ_1. At higher frequencies the magnitude of θ_3 increases and starts to have a bigger influence on θ_2.

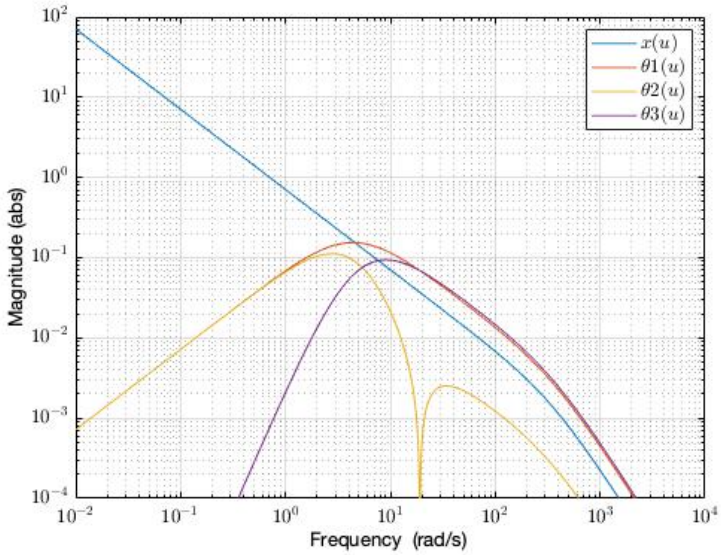

Figure 4.3: Frequency response of the system when excited by the control signal u. This signal affects all outputs of the system.

Eventually θ_2 is one of the variables that are to be minimized by the controller. At approximately 19 rad/s, where the magnitude of θ_1 and θ_3 starts to align, the magnitude of θ_2 drops drastically due to a zero in the system. This means that influencing θ_2 becomes very hard around this frequency and calls a for large control signal.
Due to coupling within the system the arms of the pendulum can only be manipulated through the dynamics of the cart. So the magnitude of the angles roll of with the magnitude of the cart at frequencies higher than 10 rad/s. Also it can be seen that at low frequencies the magnitude of θ_1 is larger then θ_3. This is natural since in order to

affect the upper joint, energy needs first to be passed through the lower joint. That is θ_3 is coupled to the system through θ_1. This is a result of having an under actuated system, in this case a system with a single actuator and 3 degrees of freedom.
From the Figure 4.3 and the discussion above it can be concluded that the system is controllable since u affects all outputs.

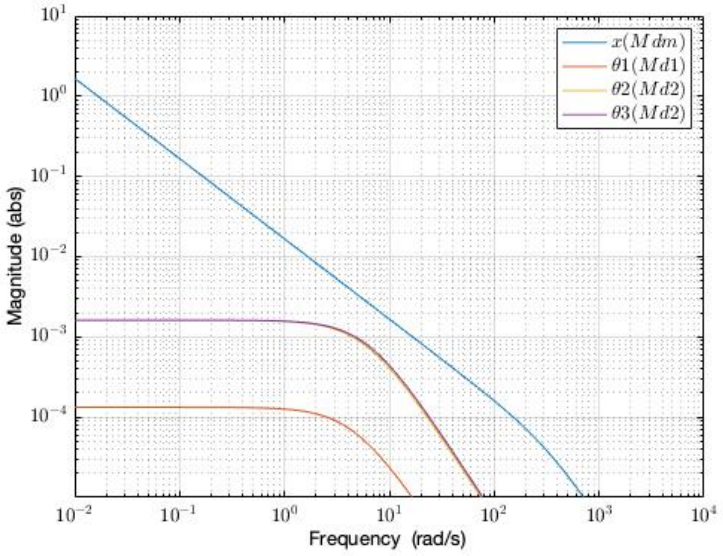

Figure 4.4: The influence of friction on individual joints. The disturbance is most apparent at low frequencies.

Taking a look at the effect of disturbances, or friction to be specific, in the system is also important since eventually disturbances need to suppressed for good control. Figure 4.4 shows the how the the outputs of the system respond to friction. In all cases the magnitude is highest at low frequencies. The effect of disturbances in the system will be investigated further in Chapter 5.4, where maximum singular values are used to evaluate the frequency response to a disturbance vector.

As already discussed Figure 4.3 indicates that the system is controllable. This has been mathematically verified with the following controllability theorem [ES08].

Controllability theorem CC3: *The Linear Time Invariant system is controllable if and only if no left eigenvectors of A exist such that:*

$$w_i^T B = 0 \tag{4.2}$$

which means that no left eigenvectors of A must be orthogonal to all columns of B.

4.3 Summary

The analysis above has confirmed that the system is unstable by looking at the eigenvalues of the system matrix A. Frequency response of the system in Figure 4.3 indicated that the system is controllable and that has been confirmed mathematically. The frequency response also shows in what frequency range the pendulum joints are most easily manipulated, that is the range in which the joints have the highest magnitude.
Analysis has also shown that the amplifier used is likely to cause trouble. The current limiting feature embedded in the amplifier slows down the response of the motor. This introduces performance limitation and reduces the range of initial conditions of the angles from which the system can be stabilized, and in worst case causes the real system not to be stablizable at all.
In case the system is initialized with the pendulum arms standing still in their vertical orientation, naturally there is no oscillation in the system. Figure 4.3 shows that at low frequencies the magnitude of the angles is very low, so influencing the angles at these frequencies calls for large a control signal and in turn high current running through the motor, which the amplifier might not be able to deliver.

The current limiter is not included in the state space model of the system. So when it comes to controller design it should be kept in mind that the actuator in the real system does not allow as swift responses as the state space model indicates.

CHAPTER 5
Controller Design

The controllers to be designed and implemented in this project are H_∞ controllers. The design process is similar to the classical loop shaping approach, but better suited to complex MIMO systems.
In this chapter the performance specification will be defined and the H_∞ optimization for robust control in the mixed sensitivity setup will be discussed. Since mathematical solution to the control problem is acquired through the use of the Robust Control Toolbox in Matlab the focus will be instead on the general setup of the problem and the design process explained.

5.1 Performance specification

In general this project is regarded as a reference tracking problem. However, due to the systems unstable nature, a priority would be to utilize the performance available in the system to stabilize the pendulum. So rather then putting high requirements on reference tracking more emphasis is made on minimizing the two joint angles.
Figure 4.3 shows that magnitudes of θ_1 and θ_3 rise from zero until they reach a peak at around 5-10 rad/s, so influencing these variables at low frequencies calls for a large control signal. When a test run is initialized frequency of oscillation in the pendulum is very low, as the arms are almost standing still. This means that starting up the system will be very demanding on the motor system. So performance should be evaluated by the controllers ability to stabilize the pendulum system from various initial conditions.

Rather then defining specific range of initial conditions that the controlled system should be able to handle, the approach is to start the design process with a very simple controller and see how much the controlled system can be improved through tuning of the design parameters.
The quality of the controllers designed will also be evaluated in terms of reference tracking, or rather the trade of between good reference tracking and robustness to initial conditions will be pointed out.

5.2 H_∞ control theory

In the discussion that follows the theory behind H_∞ control will be briefly explained and the control problem will be formulated in the general control configuration. One of the real strength of H_∞ control is how uncertainties can be included in this generalized plant, and can be used to design more robust controllers. However in this project no attempts were made to take advantage of this feature, since uncertainties are not the main concern but rather the limited amount of performance available in the system.

5.2.1 Generalized plant configuration

For H_∞ controller synthesis the plant is formulated in a so called generalized plant configuration seen in Figure 5.1. P is the generalized plant model which includes the plant G, the disturbance model G_d as well as weight functions used to influence the characteristics of the closed loop system. The input vector ω is called the exogenous input. It contains all inputs entering the system from outside, those signals are in general reference inputs, disturbances and noise. The exogenous output vector z contains the error signals to be minimized. K is the controller and v and u are the controller input and output vectors respectively[SP05].

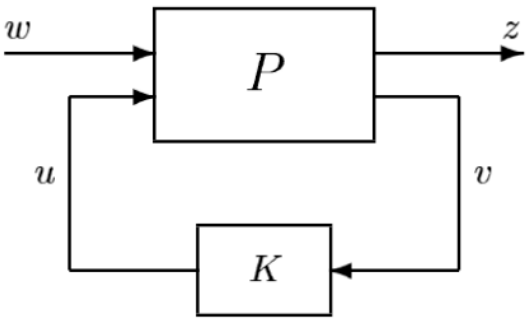

Figure 5.1: General control configuration [SP05].

The state space formulation of the generalized plant is shown in Equation 5.1

$$\begin{bmatrix} z \\ v \end{bmatrix} = P \begin{bmatrix} \omega \\ u \end{bmatrix} \tag{5.1}$$

With the control objective of this specific project in mind the vectors of the generalized plant configuration are defined and listed in Equation 5.2. The input ω consists of the reference input r_x, disturbances due to friction M_{d1}, M_{d2} and M_{dm}, along with measurement noise n_1, n_3 and n_x.

The signals that are to be minimized to obtain the control objective are contained in the output vector z. In controller design these signals will be influenced through frequency dependent weight functions. Note that including the control signal U in z allows the designer to manipulate the magnitude of the control signal at various frequencies. The scalar output of K, u, is simply the control voltage U and finally v is the controller input vector includes measurement noise.

$$z = \begin{bmatrix} e_x \\ \theta_1 \\ \theta_2 \\ U \end{bmatrix} \quad \omega = \begin{bmatrix} r_x \\ M_{d1} \\ M_{d2} \\ n_1 \\ n_3 \\ M_{dm} \\ n_x \end{bmatrix} \quad u = [U] \quad v = \begin{bmatrix} e_x \\ \theta_1 \\ \theta_3 \end{bmatrix} \tag{5.2}$$

With these vectors defined a state space representation of the generalized plant is put forward as follows.

$$\begin{aligned} \dot{x} &= Ax + B_1\omega + B_2u \\ z &= C_1x + D_{11}\omega + D_{12}u \\ v &= C_2x + D_{21}\omega + D_{22}u \end{aligned} \tag{5.3}$$

In Equation 5.3 the first output equation describes the exogenous output z. All of these outputs are either inputs or states in the state space model from 3.42. So finding matrices C_1, D_{11} and D_{12} is straight forward.

$$x^T = \begin{bmatrix} \theta_1 & \dot{\theta}_1 & \theta_2 & \dot{\theta}_2 & x & \dot{x} & i \end{bmatrix}$$

$$C_1 = \begin{bmatrix} 0 & 0 & 0 & 0 & -1 & 0 & 0 \\ 1 & 0 & 0 & 0 & 0 & 0 & 0 \\ 0 & 0 & 1 & 0 & 0 & 0 & 0 \\ 0 & 0 & 0 & 0 & 0 & 0 & 0 \end{bmatrix} \tag{5.4}$$

$$D_{11} = \begin{bmatrix} 1 & 0 & 0 & 0 & 0 & 0 & 0 \\ 0 & 0 & 0 & 0 & 0 & 0 & 0 \\ 0 & 0 & 0 & 0 & 0 & 0 & 0 \\ 0 & 0 & 0 & 0 & 0 & 0 & 0 \end{bmatrix} \tag{5.5}$$

$$D_{12} = \begin{bmatrix} 0 \\ 0 \\ 0 \\ 1 \end{bmatrix} \tag{5.6}$$

For the state equation describing $\dot{x}$ and the second output equation describing v, matrices can be taken directly form the state space model already defined in Equations 3.42-3.49 and are shown below.

$$C_2 = \begin{bmatrix} 0 & 0 & 0 & 0 & -1 & 0 & 0 \\ 1 & 0 & 0 & 0 & 0 & 0 & 0 \\ -1 & 0 & 1 & 0 & 0 & 0 & 0 \end{bmatrix} \tag{5.7}$$

$$D_{21} = \begin{bmatrix} 1 & 0 & 0 & 0 & 0 & 0 & -K_{n_x} \\ 0 & 0 & 0 & K_{n_1} & 0 & 0 & 0 \\ 0 & 0 & 0 & 0 & K_{n_3} & 0 & 0 \end{bmatrix} \tag{5.8}$$

$$D_{22} = \begin{bmatrix} 0 \\ 0 \\ 0 \end{bmatrix} \tag{5.9}$$

The difference between the two output equations is that z includes U and θ_2 which are to be minimized, whereas v includes θ_3 which is the measured angle in the upper joint of the pendulum. Also the measurement noise scale constants K_{n_1}, K_{n_3} and K_{n_x}, are included in v.

5.2.2 H_∞ optimisation

The exogenous input-output relationship for a system set up in the generalized plant configuration, shown in Figure 5.1, is $z = F_l(P, K)\omega$. The transfer function $F_l(P, K)$ is the lower linear fractional transformation of the system. The H_∞ problem evolves around finding a stabilizing controller K that minimizes the H_∞ norm of $F_l(P, K)$.

$$\|F_l(P, K)\|_\infty = \max_\omega \bar{\sigma}(F_l(P, K)(j\omega)) \tag{5.10}$$

For optimal control this may be done by iteratively solving two Ricatti equations for a system that fulfills a list of requirements (found in [SP05]). The Matlab algorithm used to find these controller fails if these conditions are not met, which means that the control problem needs to be reformulated. The peak of the maximum singular value of the resulting closed loop systems is γ and can be used as a measure of quality of control, as for an optimum controller, γ_{min} would be the lowest value of all stabilizing controllers.

Using the singular values as a measure of gain is especially convenient for MIMO systems. Since in such a system the input and output signals are vectors, and vectors have directions. So the gain of a MIMO system is not only dependent on frequency but also on the direction of the input signal.
Details about calculations of vector norms will not be put forward here, rather this discussion will be concluded with an important statement:
It can be shown that the largest gain for any input direction is equal to the maximum singular value $\bar{\sigma}$ and the smallest gain for any input direction is equal to the minimum singular value $\underline{\sigma}$ [SP05].

5.2.3 Mixed-sensitivity setup

In Equation 5.3 the state space representation for the generalized plant is put forward but the $F_l(P, K)$ matrix has not been found yet. This is most conveniently done in Matlab, but can also be acquired from the block diagram in Figure 5.2. It should be noted that this block diagram is a simplified representation of the full system, as it does not include disturbances and vector dimensions are not as defined in Equation 5.2. How ever the block diagram is useful for explaining general idea and how the weight functions, W_1 and W_2 are included in the system.

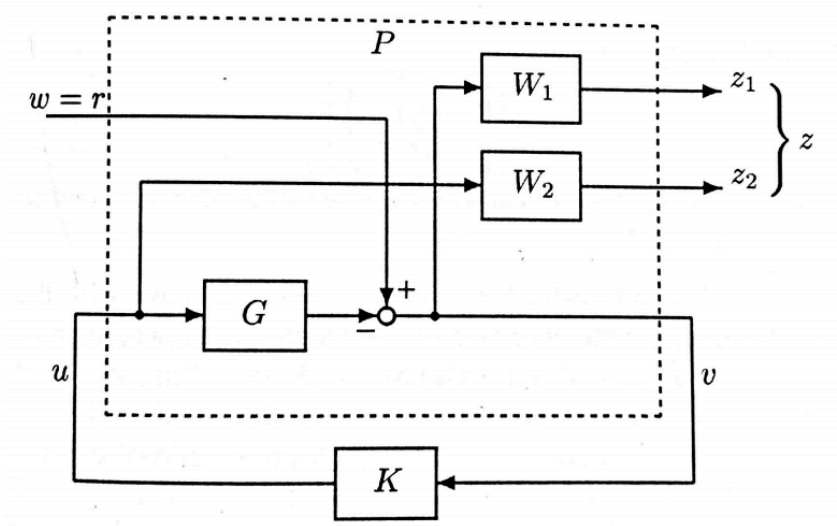

Figure 5.2: S/KS mixed-sensitivity setup [SP05].

First the relationship between inputs and outputs of P is found, which may then by put in matrix form.

$$\begin{aligned} z_1 &= W_1\omega - W_1Gu \\ z_2 &= W_2u \\ v &= I\omega - Gu \end{aligned}$$

$$\begin{bmatrix} z \\ v \end{bmatrix} = P \begin{bmatrix} \omega \\ u \end{bmatrix} \Leftrightarrow \begin{bmatrix} z_1 \\ z_2 \\ v \end{bmatrix} = \begin{bmatrix} W_1 & -W_1G \\ 0 & W_2 \\ I & -G \end{bmatrix} \begin{bmatrix} \omega \\ u \end{bmatrix} \tag{5.11}$$

The P matrix in 5.11 is split into four sub-matrices as shown below, which are then used to find the lower left fractional transformation of the system shown in Equation 5.12

$$P_{11} = \begin{bmatrix} W_1 \\ 0 \end{bmatrix}, \quad P_{12} = \begin{bmatrix} -W_1G \\ W_2 \end{bmatrix}, \quad P_{12} = I, \quad P_{22} = -G$$

$$
\begin{aligned}
F_l(P,K) &= P_{11} + P_{12}K(I - P_{22}K)^{-1}P_{21} \\
&= \begin{bmatrix} W_1 \\ 0 \end{bmatrix} + \begin{bmatrix} -W_1G \\ W_2 \end{bmatrix} K(I+GK)^{-1}I \\
&= \begin{bmatrix} W_1 \\ 0 \end{bmatrix} + \begin{bmatrix} -W_1GK(I+GK)^{-1} \\ W_2K(I+GK)^{-1} \end{bmatrix}
\end{aligned} \tag{5.12}
$$

Now with the definitions of the sensitivity function $S = (I+GK)^{-1}$, the complementary sensitivity function $T = (I+GK)^{-1}GK$ and the relationship $I = S + T$, Equation 5.12 is rewritten as such.

$$
F_l(P,K) = \begin{bmatrix} W_1(I-T) \\ W_2KS \end{bmatrix} = \begin{bmatrix} W_1S \\ W_2KS \end{bmatrix} \tag{5.13}
$$

At this stage $F_l(P,K)$ has been derived for the mixed sensitivity setup and the H_∞ optimisation method briefly explained. But before the controller K is found, through optimisation, the weight functions W_1 and W_2 have to be selected. These weight functions are frequency dependent design parameters used to shape the closed loop transfer functions.

Before continuing it is worth examining the general properties of transfer functions S, KS and T, which is most conveniently done on a general one degree of freedom feedback control system. Equation 5.14 shows how these transfer functions are derived from the block diagram in Figure 5.2.3.

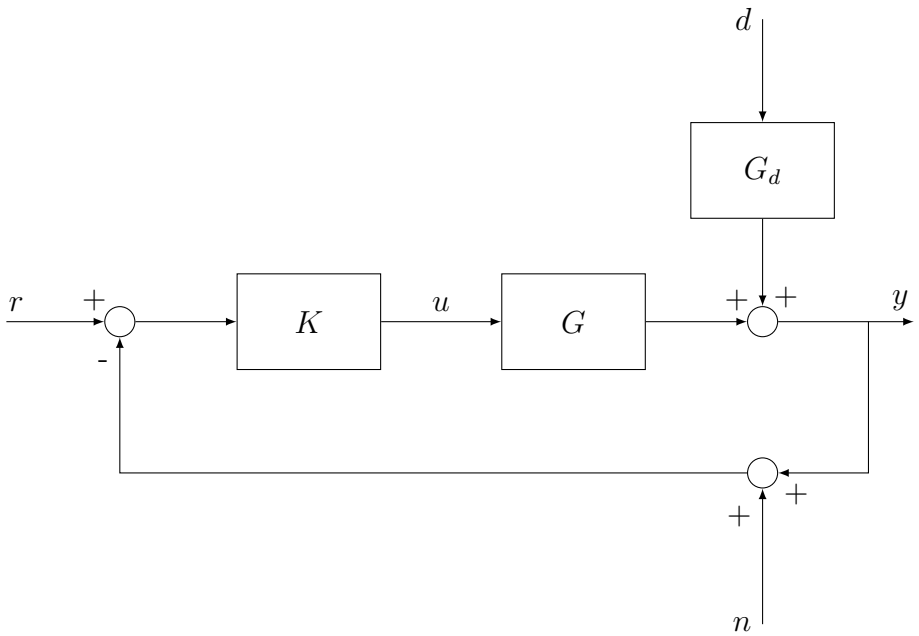

Figure 5.3: One degree of freedom feedback control.

$$\begin{aligned} y &= (I + GK)^{-1}GKr + (I + GK)^{-1}G_d d - (I + GK)^{-1}GKn \\ &= Tr + SG_d d - Tn \end{aligned} \tag{5.14}$$

It is also useful to look at the equation for the control error $e = y - r$, if the noise input is neglected. In fact the relationship in Equation 5.15 will be extensively used for analysis and design in the following chapter, where more project specific definition of S and KS, will be introduced.

$$e = -Sr + SG_d d - Tn \tag{5.15}$$

- **Sensitivity function S** is the transfer function from the reference input r to the control error e. It also describes how the disturbance vector d influences the control error. As seen in Figure 4.4 the disturbances in the system are low frequency signals. This can also be seen from Figure 5.4 which depicts the maximum singular values $\bar{\sigma}$ of the signals to be minimized when excited by d.

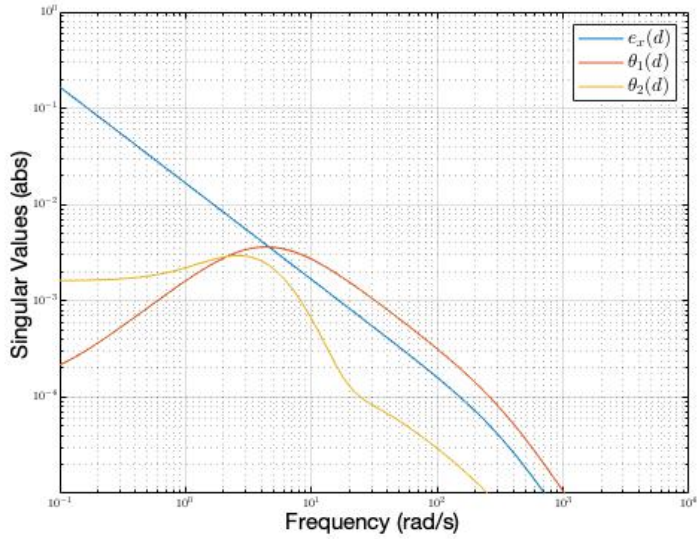

Figure 5.4: Singular values of the uncontrolled system's three outputs, when excited by the disturbance vector d. Disturbances are most apparent at low frequencies.

The magnitude at low frequencies indicates that S needs to be small at those frequencies for disturbance rejection. That is especially true in the case of the cart position error e_x which is most sensitive to disturbances.
S is also the transfer function from r to control error, which is also to be minimized at low frequencies.

- **Controller sensitivity function KS** is the transfer function from r to the control signal u, it also describes how d affects the control signal. So in order to limit the use of energy, or rather at what frequencies to use the energy, W_2 is designed as a frequency dependent shaping filter.

- **Complementary sensitivity function T** is the transfer function form r to output of the system y. Direct manipulation of T is not a part of the design process in this particular mixed sensitivity setup. How ever due to the relationship $I = T + S$, a large S inevitably means that T is small and the other way around. This is convenient since for at frequencies where disturbance rejection is required S is small and in turn $T \approx I$ so reference tracking is good. Not so conveniently a large T also means that noise easily propagates through the system, which is not desirable.

5.3 Design and closed loop analysis

Now three different controller designs are introduced, analysed and tested. Performance specifications have been defined with respect to the system´s ability to respond to different initial conditions of the two angles θ_1 and θ_2. To evaluate the performance, simulations for each design are done where the system is initialized from 300 different sets of initial conditions of the two angles θ_1 and θ_2.
Test results are presented in Figures 5.6, 5.8 and 5.10 where the red circles show the pairs of initial angels from which each controller is able to reach stability and the blue crosses show the conditions that the controller was not able to handle. All simulations are done with a discretized version of the controllers and the nonlinear simulator includes the current limiting feature of the amplifier. The discretization process is discussed in Chapter 6.

It should be clarified that in the following frequency domain analysis S_x is the transfer function from reference input to control error, and KS_x is from r to the control signal u. So rather then looking at the singular values of the overall closed loop transfer function, a SISO approach is taken to the weight design.

$$e_x = S_x r, \quad u = KS_x r \tag{5.16}$$

This approach is taken since the system is set up such that the only reference input applies to the cart position, also Figure 5.4 shows that disturbances are most apparent in the cart position. Finally, due to the coupling in the system, manipulating the frequency response of the cart naturally affects the rest of the system. So to keep things simple the focus will be on shaping two channels of the system through filters w_{p1} for the cart position error and w_u for the control signal.

$$W_1 = \begin{bmatrix} w_{p1} & 0 & 0 \\ 0 & 1 & 0 \\ 0 & 0 & 1 \end{bmatrix}, \; W_2 = w_u \tag{5.17}$$

To start this section a controller K is designed such that no weights are applied to the system's outputs. Of course this is not much of a design, but it might give a useful insight into how the weights applied later can improve the design. The controller in this initial design is called H_∞^A.

$$w_{p1} = 1, \quad w_u = 1 \tag{5.18}$$

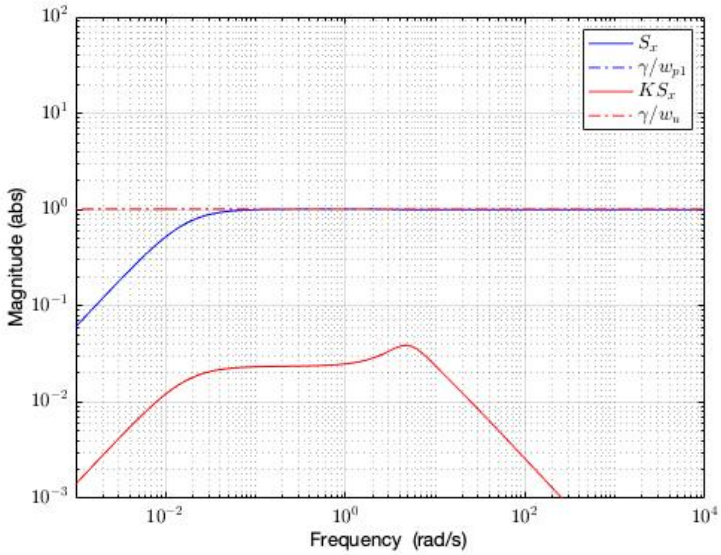

Figure 5.5: Frequency response of the system with controller H_∞^A. No weights are used to shape the closed loop system. With no attempt to shape the curves, minimizing the singular value results in $\gamma = 1$. (The blue dashed line is hidden by the red dashed line, as both lines represent 1).

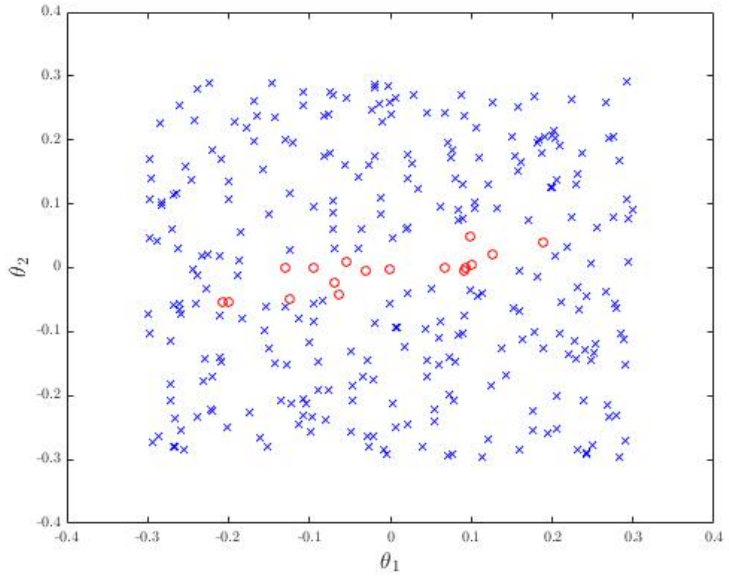

Figure 5.6: The 17 red circles represent the initial conditions from which controller H_∞^A is able to stabilize the system. Range of θ_1 is relatively big compared to θ_2, and the controller handles situations where both angles have the same sign better than the alternative.

In order to limit the magnitude of control error at low frequencies, and suppressing disturbances passing through the system, also at low frequencies, a low-pass filter w_{p1} is designed. To see the effect of w_{p1} no changes are made on w_u. The resulting controller is called H_∞^B.

$$w_{p1} = \frac{0.5s + 1}{s + 0.0001}, \quad w_u = 1 \tag{5.19}$$

With this selection of w_{p1} integral action is included in the design. A pure integrator can not be included in W_1 due to requirements for a solution of the Ricatti equations mentioned in chapter 5.3.2. So w_{p1} is designed to have a finite gain of 10^4 which will have the effect of almost eliminating steady state error. The bandwidth of the filter is chosen such that adequate disturbances rejection is gained whilst not demanding too much performance from the actuator.

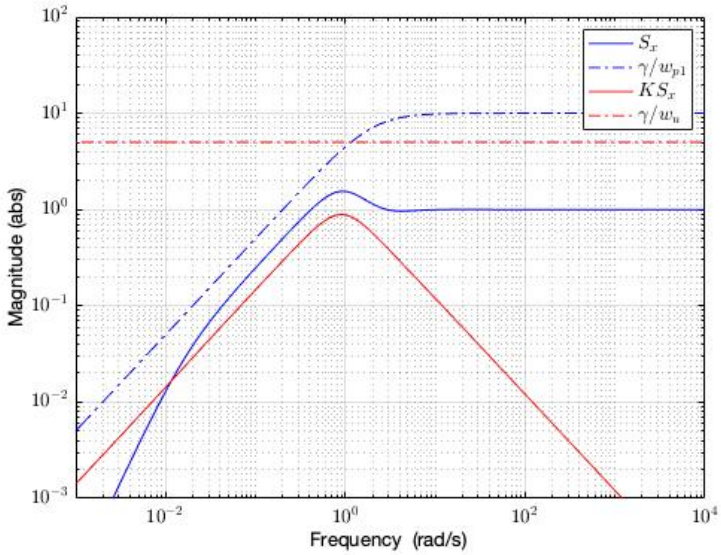

Figure 5.7: H_∞^B is designed with a low pass filter w_{p1} in order to limit the effect low frequency disturbances and control error. Notice how this filter is also limiting the KS curve at low frequencies. For this design $\gamma = 5$.

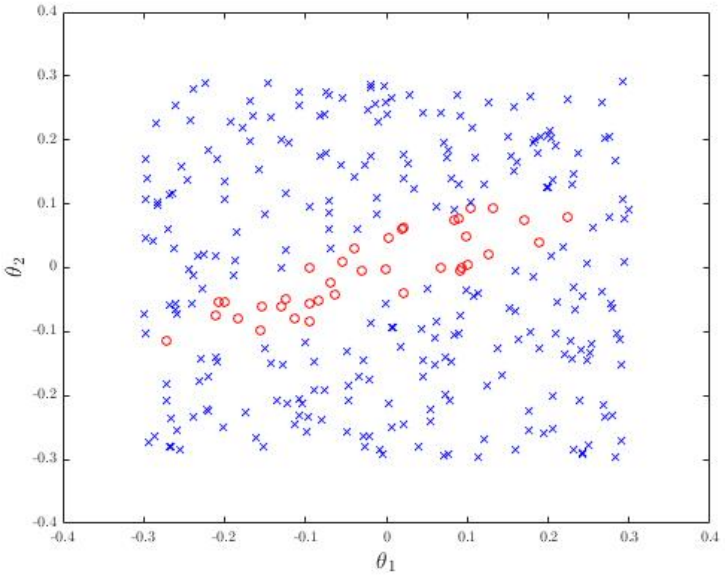

Figure 5.8: The 37 red circles show the initial conditions from which controller H_∞^B is able to stabilize the system. The trend is similar as before, the controller handles angels of the same signs better and the range of initial value of θ_1 is bigger then the range of θ_2.

In order to improve the system controller further a high-pass filter w_u is designed to shape the controller sensitivity function KS. The weight w_{p1} is kept the same as in the previous design. Figure 5.9 shows how w_{p1} affects KS at low frequencies and w_u at high frequencies which together have the effect of a band-pass filter.
Care should be take when limiting the control signal at high frequencies since the controller should be able to deal with high frequency disturbances and dynamics in the system which are not included in the system model.

$$w_{p1} = \frac{0.5s + 1}{s + 0.0001}, \quad w_u = \frac{500s + 12}{1 + 12} \tag{5.20}$$

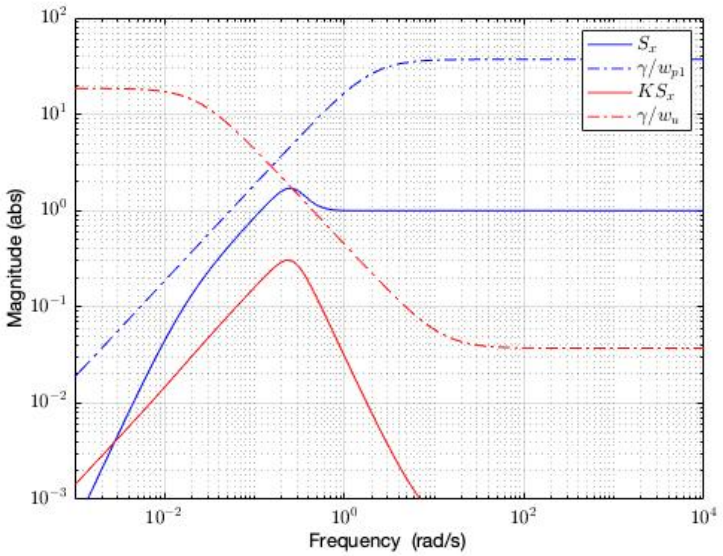

Figure 5.9: H_∞^C is designed with w_{p1} from previous design and w_u which limits the control signal at high frequencies. For this design $\gamma = 18.6$.

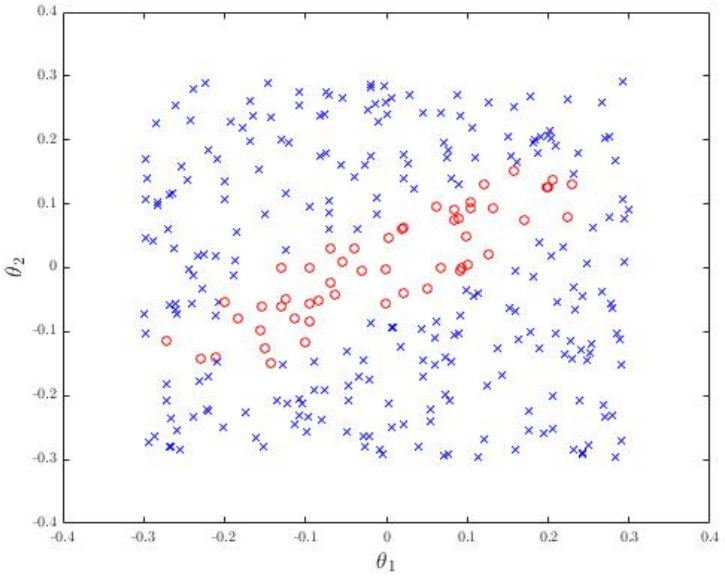

Figure 5.10: The 52 red circles show the initial conditions from which controller H_∞^C is able to stabilize the system. The trend is similar as before.

Controller H_∞^C is clearly the best one of the three designs in terms of robustness to initial conditions. It is able to stabilize the system from 52 out of the 300 initial condition tested for, compared to the 17 and 37 initial conditions which H_∞^A and H_∞^B were able to handle respectively. Judging from Figure 5.10 it appears that the H_∞^C would most likely not be able to handle more extreme initial conditions then tested for in these experiments.

Figures 5.11 show the singular values of the cart position error when the system is excited by r and $d = [M_{d1},\ M_{d2},\ M_{dm}]$. The closed loop bandwidth can be defined as the range of frequencies where control is effective. In terms of the sensitivity function S, this can be interpreted as the frequency ω_B where the magnitude reaches 0.707 from below [SP05]. At frequencies below ω_B disturbances and the tracking error are suppressed. Table 5.1 lists the bandwidths of the three designs. As seen in Figure 5.11 this definition of bandwidth does not apply to H_∞^A since in the presence of disturbances there will always be a steady state error. This is due to the lack of integral action in the design. The effect of the "almost" integration in H_∞^B and H_∞^C can be seen clearly when plotting γ/w_{p1} along side S for each designs.

Table 5.1: Closed loop bandwidth of the tree designs is the frequency where S reaches 0.707 from below.

Design	ω_B
H_∞^A	-
H_∞^B	0.05 rad/s
H_∞^C	0.3 rad/s

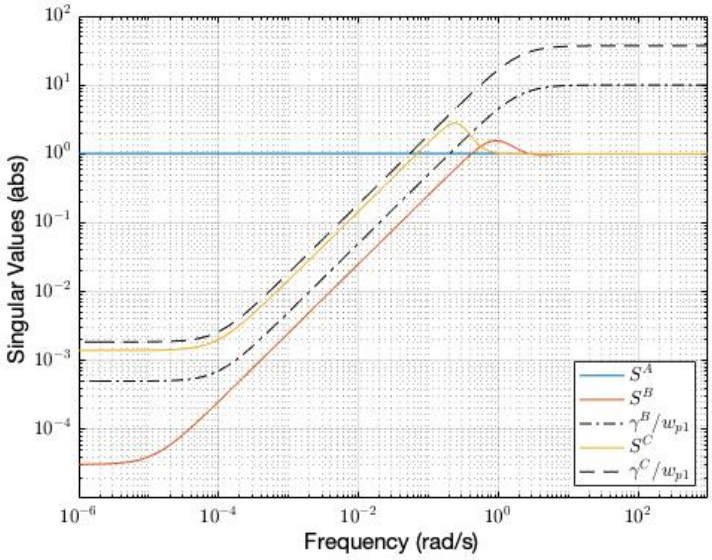

Figure 5.11: Maximum singular values of cart position error for the three designs when excited by r and $d = [M_{d1},\ M_{d2},\ M_{dm}]$.

Figure 5.12 shows how magnitude of the control signal can be manipulated over a range of frequencies. The weight w_u limits the control signal in H_∞^C design. This is done to reduce the chance of the amplifier reaching saturation and results in improved robustness to initial conditions, but performance in terms of reference tracking becomes worse compared to H_∞^B.

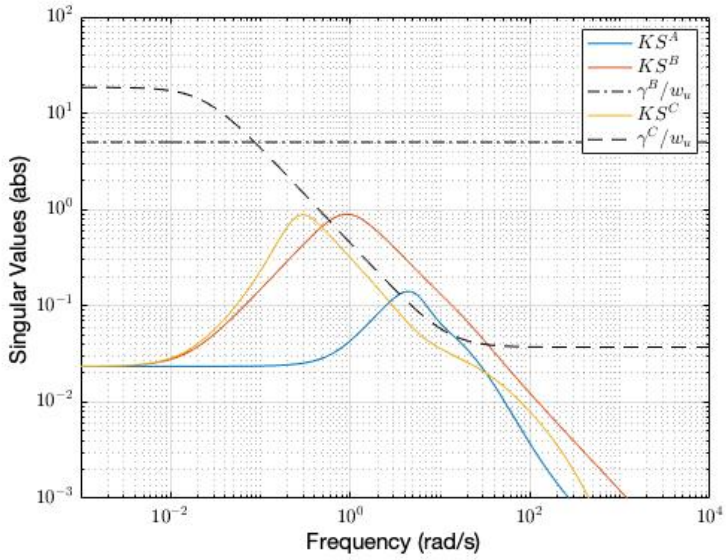

Figure 5.12: Maximum singular values of the control signal for the three designs when excited by r and $d = [M_{d1},\ M_{d2},\ M_{dm}]$.

The reason for testing the controllers ability to deal with various initial condition is that due to the current limiting feature in the motor amplifier, limited amount of performance is available in the system. So the priority in controller design is to get a stabilizing controller with this limited amount of performance available. To demonstrate this the above experiment is repeated for H_∞^C with the current limiter removed from the simulator.

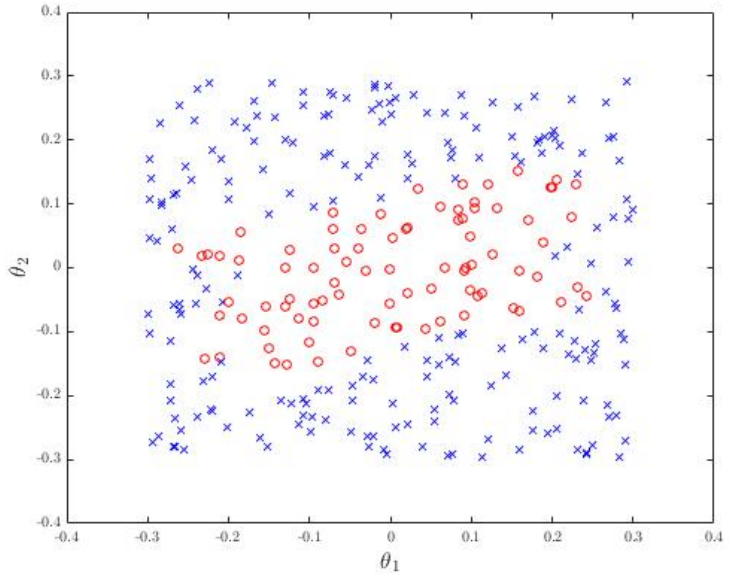

Figure 5.13: Total number of initial conditions stabilized by H_∞^C without current limiter, shown by red cricles, is 85 out of 300.

Comparing the results in Figure 5.13 where the current limiter is disabled to results in Figure 5.10 show how the performance is significantly reduced by this current limiter. The system with an ideal amplifier is stabilized form 85 initial conditions compared to 54 in the case of the actual amplifier, where both systems are controlled with the same controller.
Figure 5.14 shows a simulation of the system, with and without a current limiter, controlled with the H_∞^C controller. It can be clearly seen how the large transient spikes of the non limited system enable stabilisation whereas the current limiting feature causes the cart to run out of bounds.

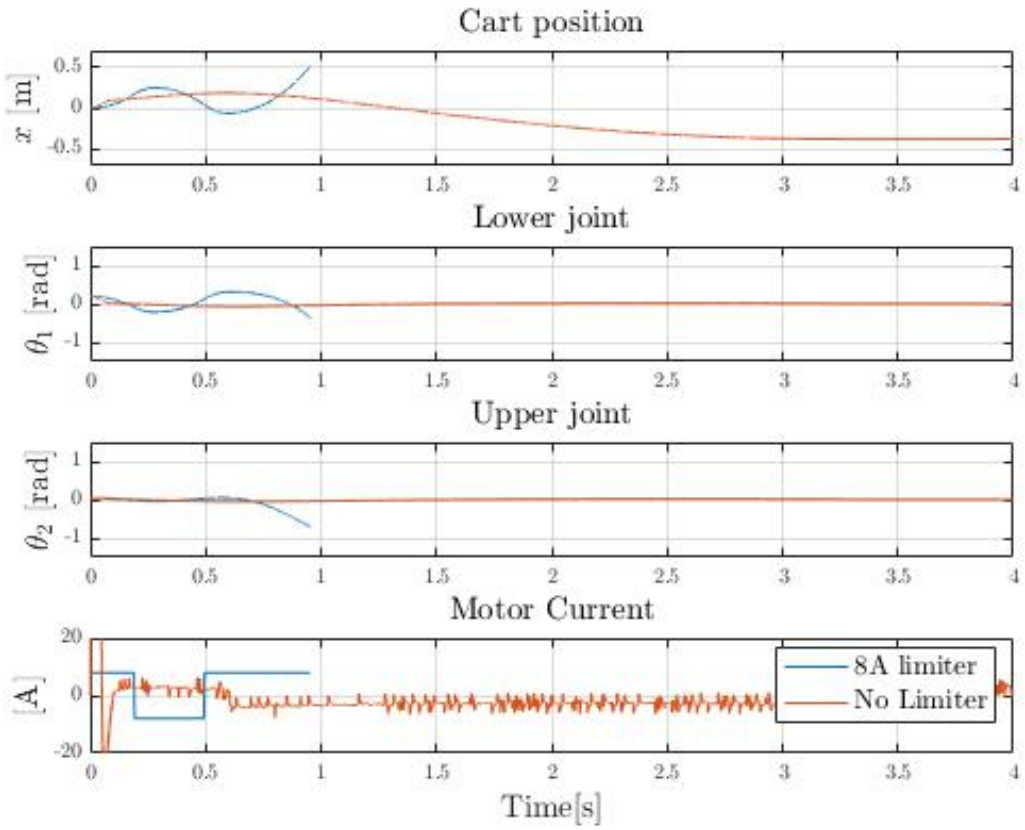

Figure 5.14: H_∞^C controller applied to the system with and without current limiter. The cart in the limited system runs out of bounds within 1 sec of simulation.

This leads to a different but an important approach to the initial conditions test results shown in Figures 5.6, 5.8 and 5.10. That is to see where the systems fail, or what causes the controller to lose control. Figures 5.15-5.18 shows results from the previous experiment. This time the initial conditions that were successfully stabilized are removed and instead the cause of failure is pointed out. Test cases where the cart reaches either end of the track is marked with a red cross, and cases where either of the joints angles get to big are marked with a blue cross.

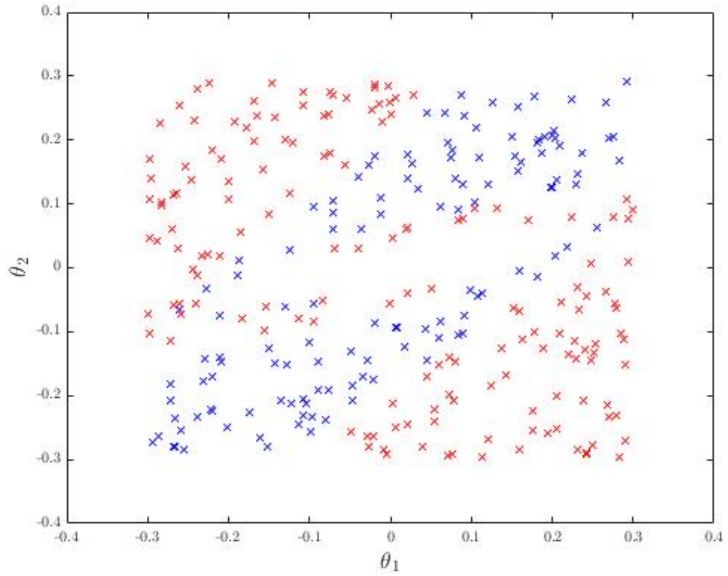

Figure 5.15: Initial conditions which H_∞^A was not able to stabilize. A red cross indicates the cart running out of bounds, and a blue cross indicate the arms falling to the sides.

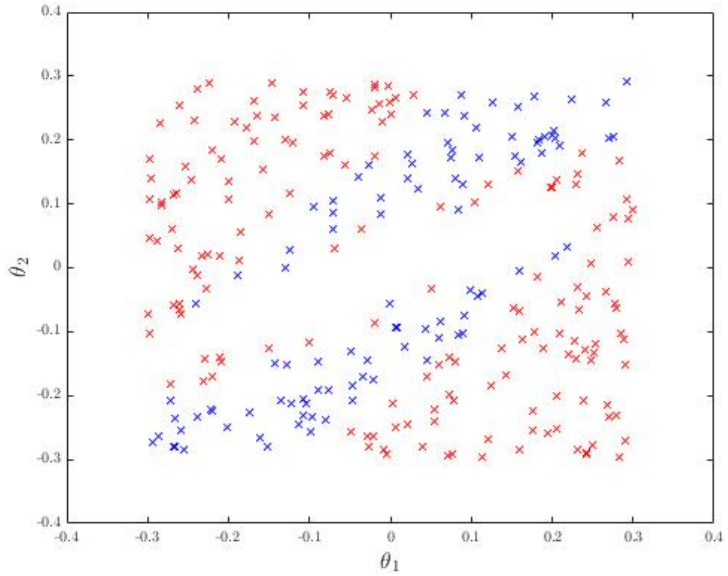

Figure 5.16: Initial conditions which H_∞^B was not able to stabilize. A red cross indicates the cart running out of bounds, and a blue cross indicate the arms falling to the sides.

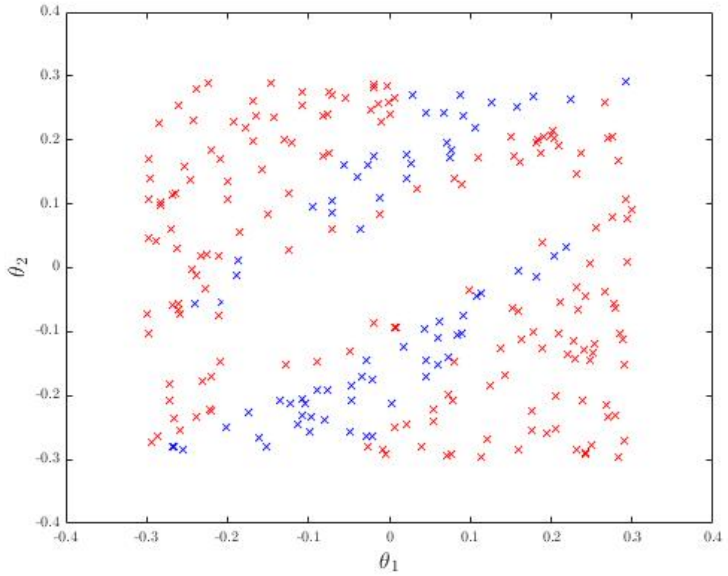

Figure 5.17: Initial conditions which H_∞^C was not able to stabilize. A red cross indicates the cart running out of bounds, and a blue cross indicate the arms falling to the sides.

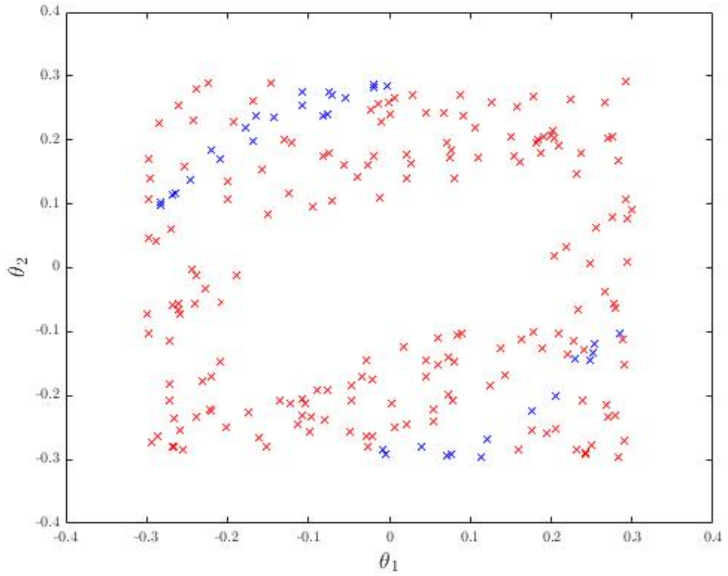

Figure 5.18: Initial conditions which H_∞^C, without current limiter, was not able to stabilize. A red cross indicates the cart running out of bounds, and a blue cross indicate the arms falling to the sides.

As the red crosses from Figures 5.15-5.18 indicate most of the failed cases the cart is running out of bounds. It is interesting to see how the blue crosses in Figure 5.17 seem to shift from almost the border of the void, close to successful area, and appear further outside in Figure 5.18.

The secondary objective of the controller is reference tracking this test of robustness to initial condition does not tell the full story of how good the controllers are. Another way to evaluate the performance of the controllers is to compare how well they do with respect to reference racking. This was done by comparing simulations from the most extreme initial condition that all controllers were able to handle.

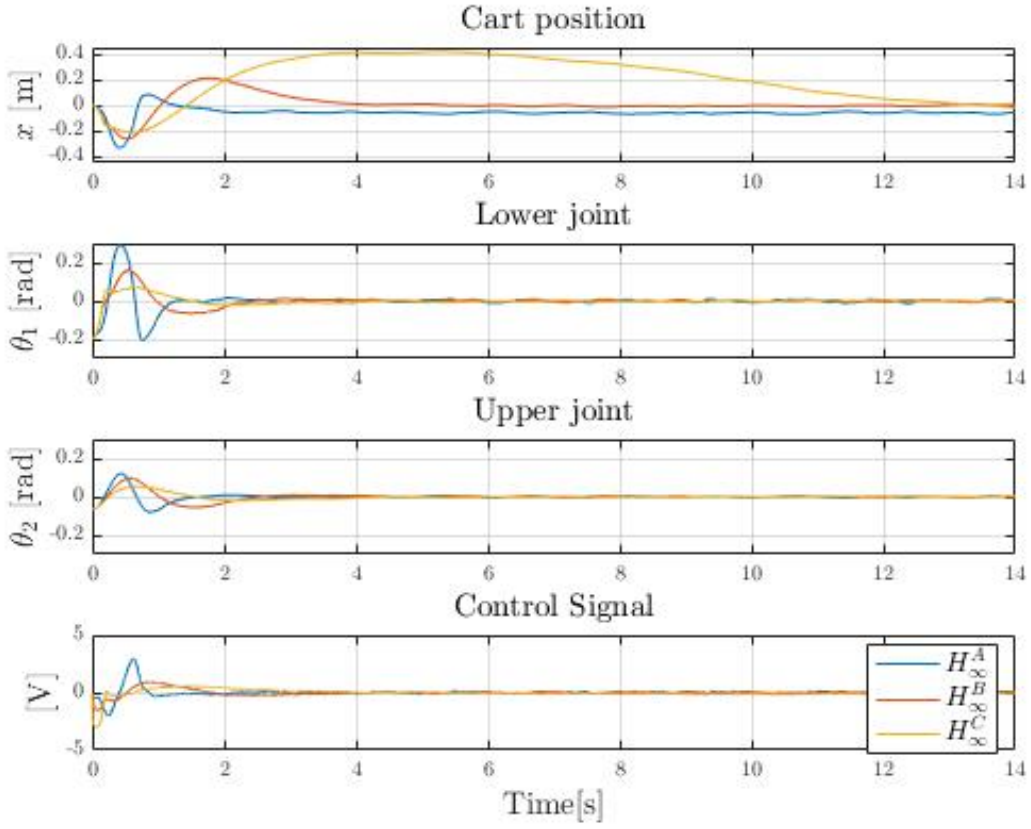

Figure 5.19: Comparison of the three systems shows that the robust controller H_∞^C shows very poor performance minimizing the cart position error in approximately 13 seconds. A steady state error is apparent in the system controller by H_∞^A.

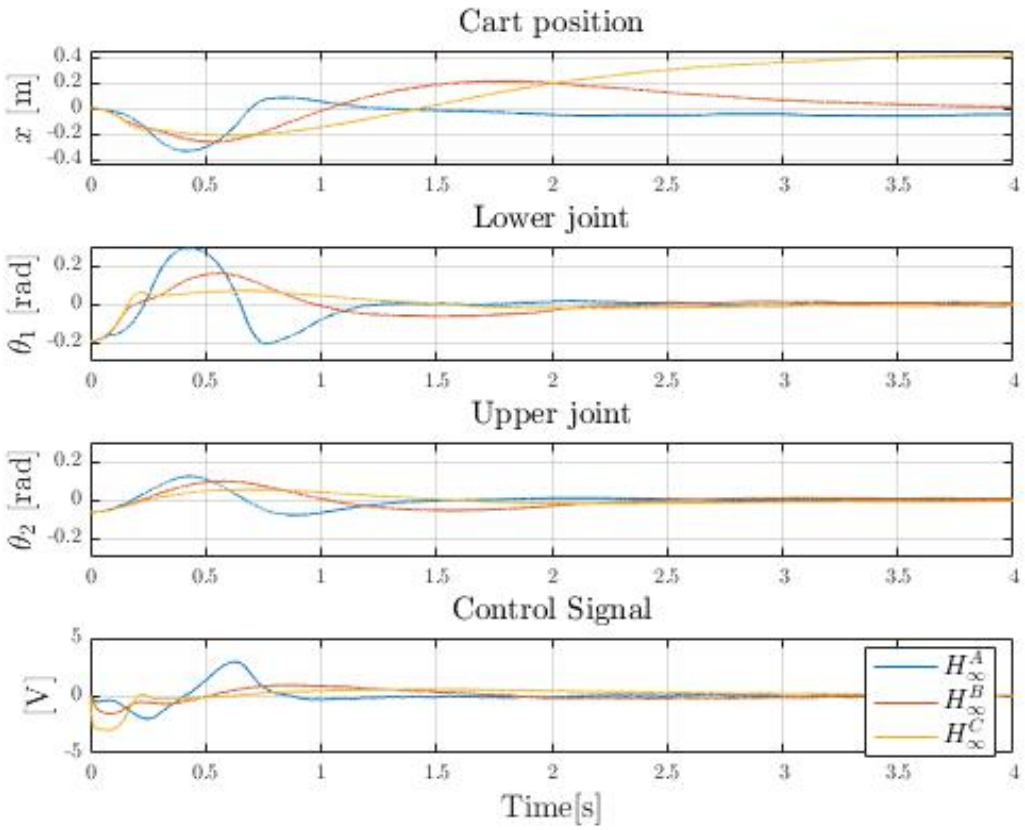

Figure 5.20: A closer look at the first 4 seconds of the previous simulation shows that H_∞^B has the best reference tracking performance while spending considerably less control energy then H_∞^A which however stabilizes the system in the shortest time.

From the simulated results shown in Figures 5.19-5.20 it can be concluded that for reference tracking H_∞^B has the best performance. It stabilizes the pendulum arms and minimizes the control error in approximately 4 seconds, while keeping the control signal fairly low.
The system controlled with H_∞^A is able to stabilize the system in about 1.5 seconds, but there is a steady state error in the cart position as the cart never reaches the reference input $r = 0$. This is due to the lack of integral action in the weight function w_{p1} for this particular design.
The integral action in H_∞^B and H_∞^C ensures that the steady state error converges to zero. So despite H_∞^A being able to stabilize the system in the shortest time it has the worst performance in reference tracking, just as it was least robust to initial conditions of the three controllers.

5.4 Summary

The process for controller design described in this chapter, really does not end here. The design parameters w_{p1} and w_u can most likely have better designs, also further tuning is expected when it comes to implementing the controller on the real system. The weight matrix W_1 might as well include weights on θ_1 and θ_2 also uncertainty analysis would be a natural step forward for further development.
The discussion above how ever describes the design process for this project. It has been shown how controllers can be systematically improved in order to obtain or get closer to the control objective. It has been shown how single weight on the cart position error the w_{p1} improves the performance in terms of all outputs and how w_u can be used to utilize the available performance in the appropriate frequencies.
The impact of the current limiter of the amplifier has been pointed out a few times all ready, and yet again it has been shown how this is degrading the performance of the system. An alternative to replacing the amplifier might be to increase the length of the track or perhaps to shorten the arms of the pendulum. In any case implementing a controller on the Test-Rig in its current condition is going to be very demanding.

CHAPTER 6

Real Time Programming

In this chapter the C program written for this project will be described as well as the process of data acquisition. Terms related to real-time programming such as threads, task management and scheduling will be briefly explained and the software implementation of a controller in a state space form will be described.
The PC used for this project had a real-time operating system called RTAI which offers many useful functions for real time programming. Some of these functions were utilized in this project and the most important ones will be explained in this chapter. Figure 6.1 is a diagram showing the flow of data between the Test-Rig and the PC.

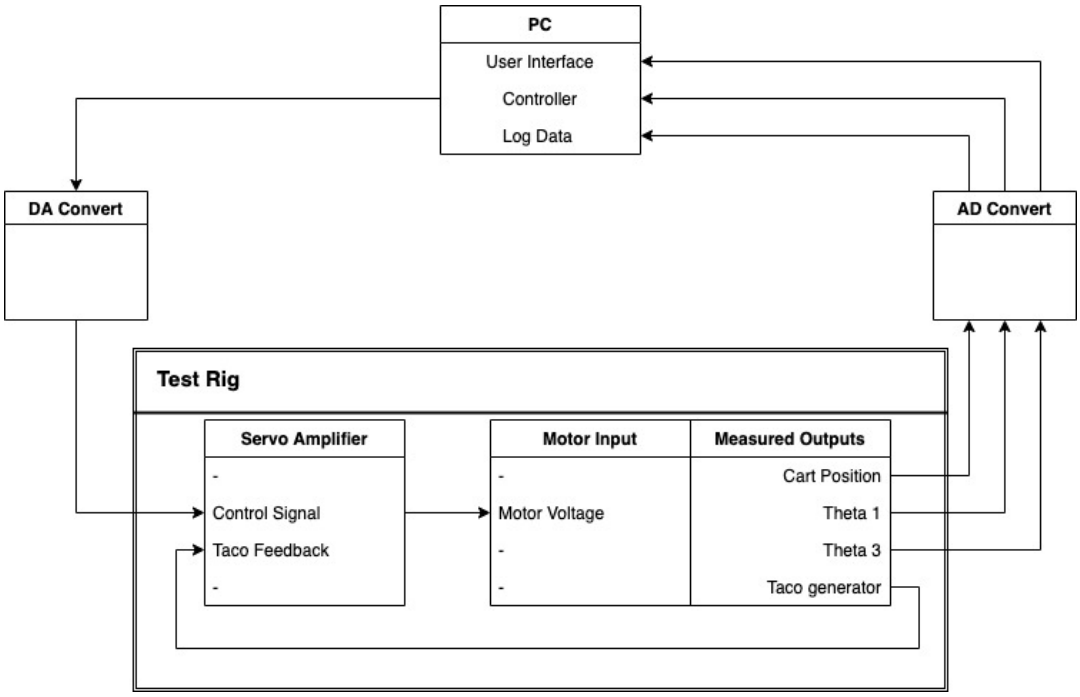

Figure 6.1: Overall system diagram.

6.1 Data acquisition

As seen in Figure 6.1 the PC receives the three controller input signals. These analog signals are filtered, to reduce measurement noise, before they are discretized by the AD-

Converter. The controller output how ever is sent unfiltered through the DA-Converter to the servo amplifier.
The filter circuit for the angle measurements is a simple RC-filter that includes a signal amplifier and an offset adjustment. The circuit for the cart measurement is also a RC-filter, but without amplification and offset adjustment. A diagram of these circuits can be seen in Appendix C.

The Comedilib library, used as an interface for the AD/DA converters, offers a function call that returns the measured values in voltages. The potentiometers used are fairly linear so converting the measured voltages to appropriate units is straight forward using the data form Table 6.1 and Equation 6.1. The offset adjustment in the angle measurement circuit is tuned such that both angles read zero in fully vertical orientation.

Table 6.1: Full range of the measured values in their physical units and the corresponding values in voltages are used to calculate the conversion factor.

	Physical Range	**Measured Voltage**	**Conversion Factor**
x	1 m	5.1 V	0.196 $\frac{m}{V}$
θ_1	2.69 rad	9.49 V	0.285 $\frac{rad}{V}$
θ_3	3.14 rad	8.7 V	0.361 $\frac{rad}{V}$

$$\textbf{Conversion Factor} = \frac{\textbf{Physical Range}}{\textbf{Measured Voltage}} \tag{6.1}$$

Even after filtering the signals there is still some noise apparent in the measurements. This is not considered to be a problem since the noise magnitude is around $1.2mV$, which translates approximately to 3.5×10^{-4}rad for the angle measurements.
Since the control signal has volts as its unit, the signal can be passed to the amplifier through the DA-Converter with out any conversion.

6.2 Software

The program written for this project consists of three threads running simultaneously. Each thread is carrying out a specific task. These tasks get assigned different priority levels, depending on how sensitive the tasks are to lagging. The task that executes the controller algorithm has the highest priority since the controller is discretized for a specific sampling frequency. Deviations in this frequency are to be minimized since they do affect the gain magnitude of the controller. The user interface task is far less sensitive to variations in its period it gets assigned the lowest priority. By running a priority based scheduler the operating system interrupts a low priority task to execute

a high priority task.
Figure 6.2 is a diagram of the program, showing the most important function calls of each thread.
The *main()* thread is the only non-periodic thread, as each of its objectives only need to be done once. These objectives are to fetch the controller state space matrices from a .txt file, later used for calculations in the controller algorithm, and to initialize and terminate the two periodic threads.

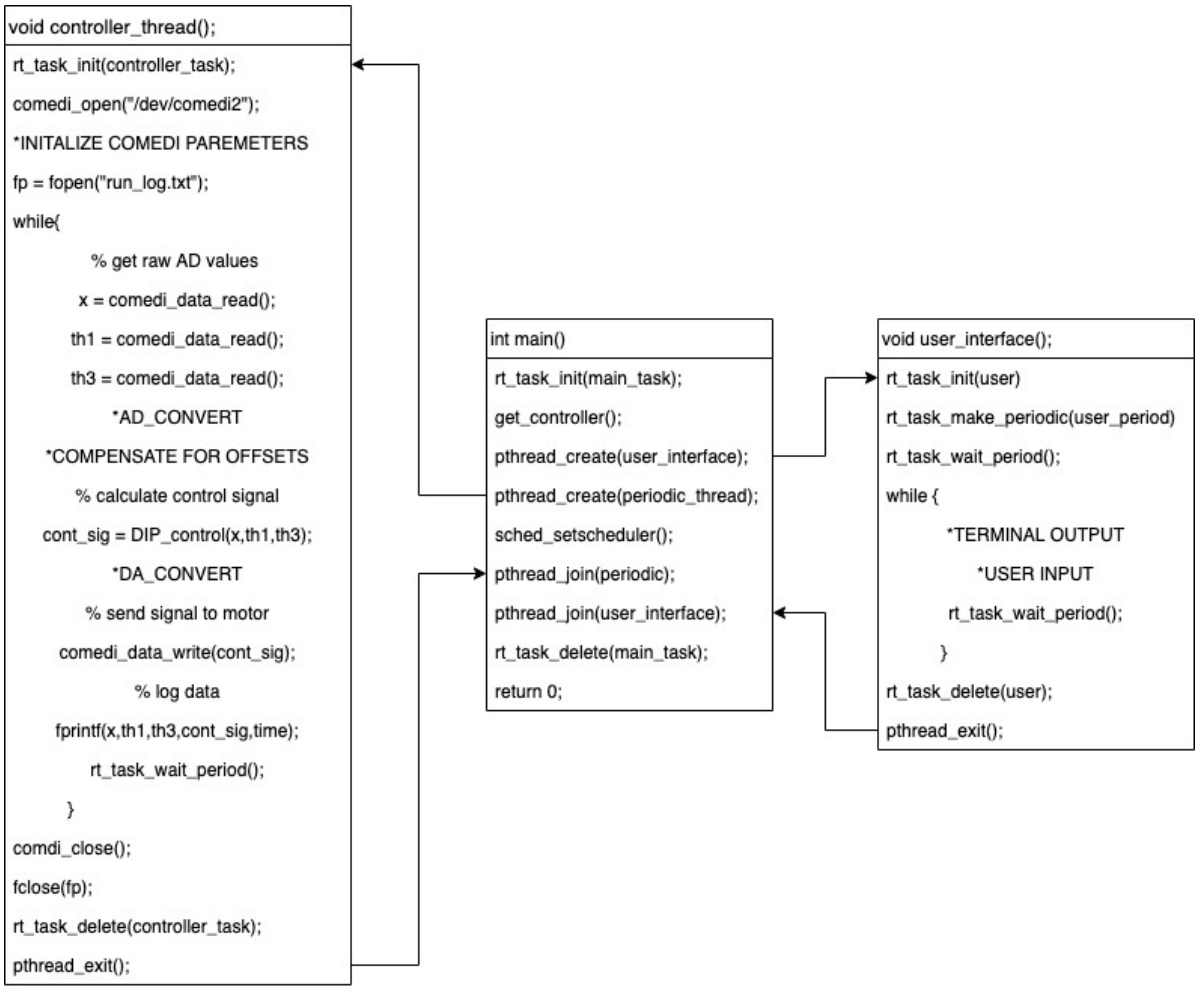

Figure 6.2: The three threads of the software. Most important function calls of each thread are shown.

The *user_interface()* thread has low priority and is running periodically. Its objective is to interact with the user via the computer display and the keyboard. It allows the user to start and stop the controller process as well as to change the reference input in real time. Interaction with humans usually does not require threads to run at more then 10-20Hz, in this case the *user_interface()* is running at 20Hz with out any problems.

The *controller_thread()* has the highest priority as it implements the controller algorithm which is very sensitive to variations in sampling frequency. This thread interacts with the AD/DA converters utilizing the *comedilib.h* library, and logs the test run data into a .txt file with functions from the *stdio.h* library. The running frequency of the *controller_thread()* is 1000Hz since it needs to match the sampling frequency of the discrete controller.

6.3 Discrete controller

The controller design in previous chapter gave a continuous time controllers that need to be discretized for digital implementation. Converting a continuous time system to a discrete one is called a Z-transform. Details of Z-transform will not be discussed here, however the choice of sample time T_s will be explained.

Generally the sampling period is determined by Equation 6.2, where $f_B = \omega_B/(2\pi)$ and ω_B the closed loop bandwidth of the system [DB17]. Table 5.1 lists the bandwidth of the three designs, with H_∞^B having the highest bandwidth of $\omega_B = 0.3\frac{rad}{s}$. However this definition of bandwidth might not be suitable for finding an appropriate sampling period.

$$T_s \leq \frac{1}{10 f_B} \tag{6.2}$$

A more reasonable definition of bandwidth for the selection of sampling period is found by looking at Figure 6.3. It shows the singular values of all outputs of the closed loop system for the three designs. It can be seen that dynamics of θ_1 and θ_3 start to roll of after approximately $8\frac{rad}{s}$.

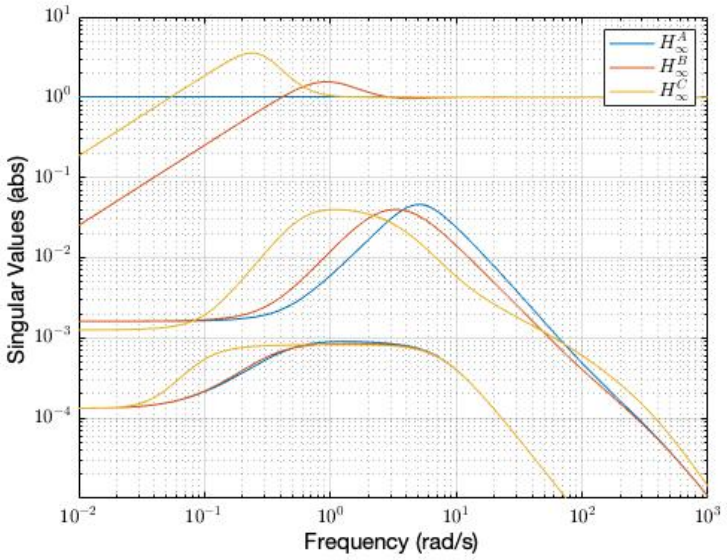

Figure 6.3: Singular values of all outputs e_x (the sensitivity function S_x), θ_1 and θ_3 of the three designs when excited by the input vector ω.

So re-defining $\omega_B = 8\frac{rad}{s}$ and applying Equation 6.2 gives a minimum sampling period.

$$T_s \leq 0.076 \tag{6.3}$$

From the discussion above it is concluded that $Ts \leq 0.076$ is sufficiently small sampling period, but since the PC has more than enough computing power the sampling period is chosen to be even smaller.

$$T_s = 0.001$$

Having chosen the sampling period the discrete controller K_d is found using the Matlab function *c2d*, which takes as input the sampling period T_s and the continuous time controller K.

6.4 Discrete implementation

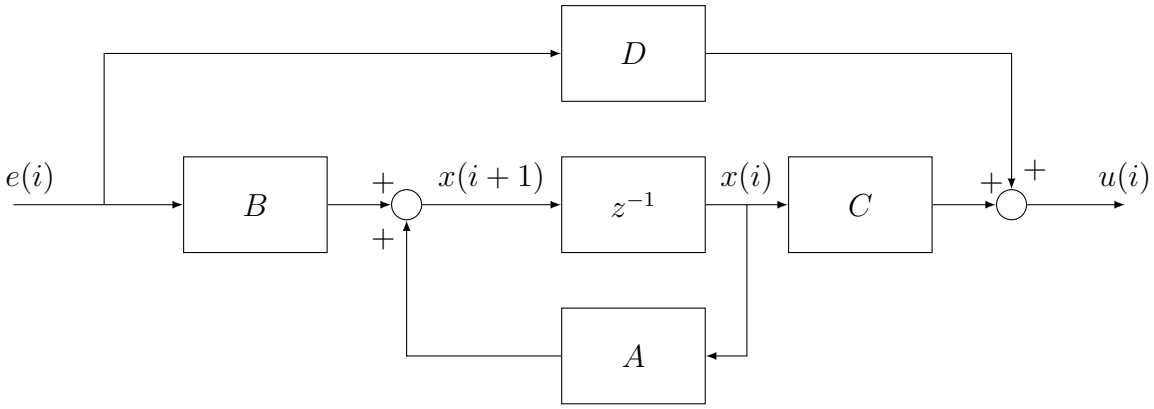

Figure 6.4: The discrete controller K_d can be realised as a state space space model.

The discrete controller K_d is implemented as a state-space model shown in Figure 6.4. The dynamical order of the controller depends not only on the order of the plant, but also on the weight functions used to in the design process. If a weight function from the controller design process has an integrator, it will be included in the controller. So the size of the state vector $x(i)$ varies between controller designs, and depends on the number of integrators. In this project the error $e(i)$ is a $[3 \times 1]$ vector and $u(i)$ a scalar. Implementing this in a program is actually quite simple and the general scheme is shown below, where $DUMMY$ and W are temporary variables [MLL82].

1. $DUMMY = Cx(i)$
2. Get the error: $e(i)$
3. $u(i) = DUMMY + De(i)$
4. Send control signal: $u(i)$
5. $W = W + Ax(i)$
6. $x(i + 1) = W + Be(i)$
7. $W = 0$

Executing these operations in a C program is not as straight forward since the matrix algebra can get a bit complex. The function *DIP_control()* in Appendix E shows the software implementation of the controller algorithm in full detail.

6.5 Verification

It is obviously very important that the controller is implemented correctly in the C program. A simple experiment to check this is to compare the step response of the discrete controller in Matlab with a step response of the same controller implemented in the C program. Figure 6.5 shows the controller outputs for the first 10 iterations of the control algorithm when a step signal is applied to one of the controller inputs.

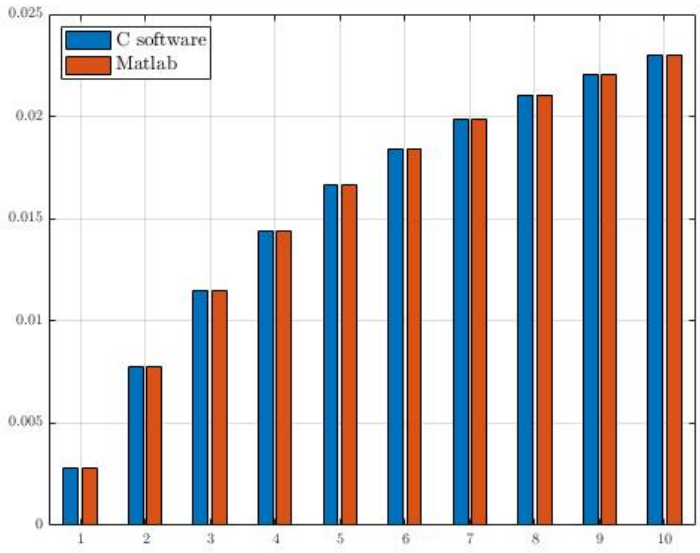

Figure 6.5: A step response of a discrete controller K implemented in Matlab and in C software. First 10 iterations indicate that the controller is implemented correctly in C software.

It is also relevant to compare the discrete controller K_d with the corresponding continuous controller K in frequency domain. Figure 6.6 shows the frequency response of individual channels of K and K_d. As required K_d has the same response as K at the desired frequency range. Discrete control is effective up until the black line, indicating the Nyquist frequency of the sampled controller. The Nyquist frequency is related to the sampling period T_s and can be calculated in radians per second with Equation 6.4, it is found to be $f_N = 3141.6\frac{rad}{s}$.

$$f_N = 0.5\frac{2\pi}{T_s} = \frac{\pi}{T_s} \tag{6.4}$$

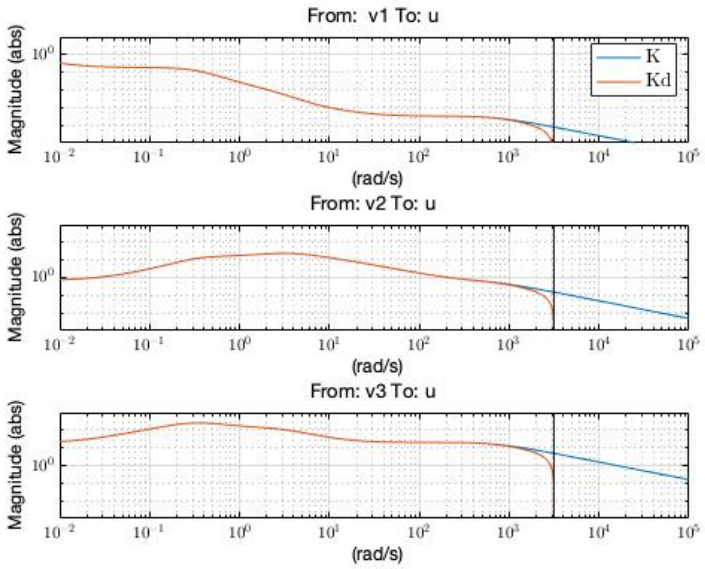

Figure 6.6: Frequency response of K and K_d. The discrete controller sufficiently represents the continuous controller at frequencies below the Nyquist frequency indicated by the black lines..

6.6 Summary

The RTAI operating system serves this project very well. The task management is fairly simple, as there are only two periodic threads, and the fixed priority scheduling scheme is adequate. Writing the program in C programming language might seem a bit intimidating at first. But the advantage is that in such a low level programming language the program becomes very transparent and can be made very efficient in execution, which is important for real-time programming and troubleshooting.
It has verified that the discrete controller K_d sufficiently approximates the continuous time controller K in the desired frequency range and that the software implementation of the controller algorithm gives the same controller outputs as the Matlab implementation.

An experiment that would have been in order is to test whether the sampling period defined T_s actually matches the execution time of the software implementation of the controller loop. It is very important that the period of the controller algorithm are as close as possible to the period used for discretization, since deviations from the theoretical period will affect the magnitude of the control signal. Unfortunately lack of time did not allow this experiment to be carried out.

Due to lack of testing it is hard to evaluate whether the digital implementation aspect of this project is a success. The main objective of stabilizing the real system was not reached, how ever the discussion above indicates that many of the sub-objectives of the

digital implementation were reached.

CHAPTER 7

Conclusion

To broadly summarise the work done and described in this thesis the main objective was not reached. That is no successful attempts were made to stabilize the inverted double pendulum. However in terms of the sub-objectives listed in Chapter 1 the results are much more positive.

7.1 Summary

A mathematical model has been derived and implemented as a nonlinear simulator. The same model has been used to derive a state space model of the system used for system analysis. The state space model was also used to acquire the generalized plant model eventually formulated in the mixed-sensitivity setup for controller design. The model has been verified to some extent, and a suspected flaw has been pointed out both mathematically and from inspection of simulated results.

This suspected flaw has been the cause of considerable confusion. Especially since in the previous work of Poulsen, on which this project is based on, this seems not to have been an issue since he was in fact successful in stabilizing the system. An alternative approach to modelling the system was carried out in Appendix A. Comparison of these two models shows that the alternative model better represents the physical system, at least with respect to the frame of reference defined in the principal diagram of the system.
Since the origin of this suspected error has not been found it is not justifiable to state that the model is wrong, in fact it has been shown that both models represents the dynamics of the system very well in every aspects besides the mismatch in directions. It was therefore concluded that the model is fit for system analysis and controller design.

Analysis of the uncontrolled system revealed that the system is controllable, which is not always the case for under-actuated system. Analysis also confirmed what intuitively was suspected, that the system is unstable by nature. Another important observation is how disturbances affect the system at low frequencies, that information proved valuable in controller design.
The issue with the current limiting feature of the motor amplifier was addressed in Chapter 4. It was shown how this feature degrades the motor systems ability to deliver the required power to the pendulum system. This might in fact be the biggest obstacle

faced in this project. The limited amount of performance available in the system calls for careful consideration on where, in terms of frequencies, to spend the control energy available.

With the shortcomings of the motor sub-system in mind, the controller design was approached in a mixed-sensitivity setup for H_∞ controller synthesis. This approach allowed shaping of the sensitivity function S for frequency dependent disturbance rejection, and the controller sensitivity function KS for appropriate usage of control energy. It has been shown how stabilizing controllers may be found, and systematically improved by appropriate selection of weight functions.
The resulting closed loop systems were analysed and evaluated in terms of the control objectives. The controllers designed proved to successfully stabilize the simulated system, but showing different performances in terms of robustness to initial conditions, reference tracking and settling time.

Software implementation of the controller is described in Chapter 6 as well as the process of data acquisition. It has been verified that the controller algorithm is correctly implemented in the software. The discrete system has been analysed and successfully tested in simulation. The objective of software implementation is therefore reached in some extent but not completely.

From the discussion above it is clear that there is still work to be done in order to meet project ultimate objective. The main obstacles are the limitations of the amplifier and perhaps loose ends in software implementation. The former issue can only be rectified by another amplifier, whereas more time for troubleshooting and improvements would likely solve the latter issue. It is therefore in order to put forward some suggestions for future work.

7.2 Future work

Although the controller algorithm is correctly implemented in software, it does not mean that other aspects of the software are flawless. Further experiments and testing would be ideal to evaluate and improve the software. Execution time of the controller algorithm should be verified, and any confusion regarding mismatch of direction definitions in the real system and in the model should be cleared up.
If, as suspected, the model derived in Chapter 3 is in fact not entirely correct, there are a number of scenarios where this flaw might be compensated for. The polarity of the motor terminal, the cart position potentiometer or the terminals of the potnetiometers measuring the joint angles might be inverted. This might also be corrected in software by simply inverting signs measurement or output signals. Ideally the source of this mismatch between the two models should be found, and can be regarded as future work.

Appendices

APPENDIX A

Euler-Lagrange Modelling

A.1 System modeling

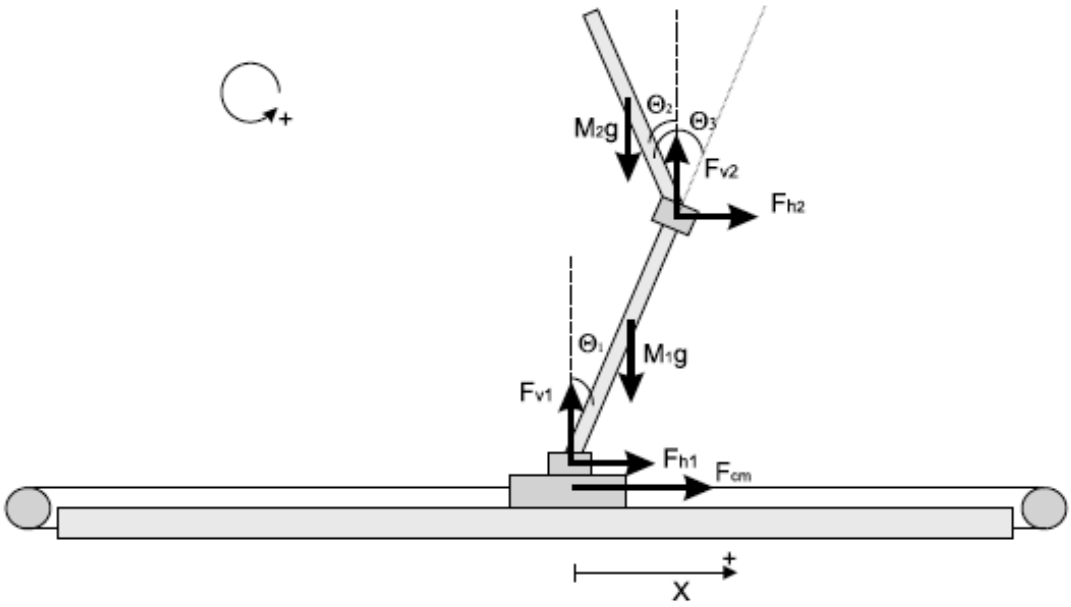

Figure A.1: Principal diagram of the double inverted pendulum.

A.1.1 Pendulum system

For the purpose of controller design, the pendulum system needs to be modeled mathematically. This can be done by using the Lagrange method. Equation A.1 is the Euler-Lagrange equation where L is the difference between the systems kinetic energy and and potential energy shown in EquationA.3-A.4.
Constant m_0 represents the mass of the cart, m_1 and m_2 are the masses of the lower arm and upper arm (note that here masses in the system are lower case m_i, opposed to upper case M_i representation in the Chapter 3 and in Appendix B). The length of lower

arm is l_1, l_{1cm} is the distance from bottom joint to lower arms center of mass and l_{2cm} is the distance from top joint to top arms center of mass.

$$\frac{\mathrm{d}}{\mathrm{d}t}\frac{\partial L}{\partial \dot{q}_i} - \frac{\partial L}{\partial q_i} \tag{A.1}$$

$$L(\theta_1, \dot{\theta}_1, \theta_2, \dot{\theta}_2, \dot{x}) = K - P \tag{A.2}$$

$$K = \frac{1}{2}m_0 V_0^2 + \frac{1}{2}m_1 V_1^2 + \frac{1}{2}m_2 V_2^2 + \frac{1}{2}I_1\dot{\theta}_1^2 + \frac{1}{2}I_2\dot{\theta}_2^2 \tag{A.3}$$

$$P = m_1 y_1 g + m_2 y_2 g \tag{A.4}$$

Equations A.5-A.7 are the position of the three masses as a function of time derived from Figure A.1. Position of the car is $\bar{p}_0(t)$, the lower and upper arms centers of mass are $\bar{p}_1(t)$ and $\bar{p}_2(t)$ respectively.

$$\bar{p}_0(t) = \begin{bmatrix} x\,(t) \\ 0 \end{bmatrix} \tag{A.5}$$

$$\bar{p}_1(t) = \begin{bmatrix} x\,(t) - l_{1cm}\sin\left(\theta_1\,(t)\right) \\ l_{1cm}\cos\left(\theta_1\,(t)\right) \end{bmatrix} \tag{A.6}$$

$$\bar{p}_2(t) = \begin{bmatrix} x\,(t) - l_1\sin\left(\theta_1\,(t)\right) - l_{2cm}\sin\left(\theta_2\,(t)\right) \\ l_1\cos\left(\theta_1\,(t)\right) + l_{2cm}\cos\left(\theta_2\,(t)\right) \end{bmatrix} \tag{A.7}$$

In order to find the velocity of the three masses we take the time derivative of the three position vectors. The magnitude of the velocity vectors is found using conventional vector norm, and finally squaring the results for inserting into EquationA.3 gives,

$$V_0^2 = \dot{x}^2 \tag{A.8}$$

$$V_1^2 = \dot{x}^2 - 2l_{1cm}cos(\theta_1)\dot{x}\dot{\theta}_1 + l_{1cm}^2\dot{\theta}_1^2 \tag{A.9}$$

$$V_2^2 = \dot{x}^2 + 2l_1 l_{2cm}cos(\theta_1 - \theta_2)\dot{\theta}_1\dot{\theta}_2 - 2l_1 cos(\theta_1)\dot{x}\dot{\theta}_1 - 2l_{2cm}cos(\theta_2)\dot{x}\dot{\theta}_2 + l_1^2\dot{\theta}_1^2 + l_{2cm}^2\dot{\theta}_2^2 \tag{A.10}$$

For the potential energy we only need the vertical component of the position vectors, and insert them into Equation A.4.

$$y_0 = 0 \tag{A.11}$$

$$y_1 = l_{cl}cos(\theta_1) \tag{A.12}$$
$$y_2 = l_1cos(\theta_1) + l_{2cm}cos(\theta_2) \tag{A.13}$$

Inserting Equations A.5-A.10 into the kinetic and potential energy equations we have the Euler-Lagrange equation L and are ready to perform the derivatives in Equation A.1. This has to be done for each variable x, θ_1 and θ_2.

$$\frac{\mathrm{d}}{\mathrm{d}t}\frac{\partial L}{\partial \dot{x}} - \frac{\partial L}{\partial x} = F_p \tag{A.14}$$

$$\frac{\mathrm{d}}{\mathrm{d}t}\frac{\partial L}{\partial \dot{\theta}_1} - \frac{\partial L}{\partial \theta_1} = \tau_1 \tag{A.15}$$

$$\frac{\mathrm{d}}{\mathrm{d}t}\frac{\partial L}{\partial \dot{\theta}_2} - \frac{\partial L}{\partial \theta_2} = \tau_2 \tag{A.16}$$

Now Equation A.14 gives F_p, the horizontal force that the pendulum exerts on the belt that connects the chart to the motor system. EquationA.15-A.16 give the dynamics of the two joints of the pendulum. Variables τ_1 and τ_2 are the friction in these two joints, which each consist of viscous friction and Coulomb friction.

$$\tau_1 = K_{v1}\dot{\theta}_1 + K_{d1}M_{d1} \tag{A.17}$$
$$\tau_2 = K_{v2}\dot{\theta}_2 + K_{d2}M_{d2} \tag{A.18}$$

Rewriting Equations A.14-A.16 in terms of the linear acceleration components H_{ij}, the components related to angular acceleration M_{ij}, the Coriolis and centrifugal components K_i and terms related to gravity G_i.

$$H_{11}\ddot{x} + M_{11}\ddot{\theta}_1 + M_{12}\ddot{\theta}_2 + K_1(\theta_1, \dot{\theta}_1, \theta_2, \dot{\theta}_2) = F_p \tag{A.19}$$

$$H_{21}\ddot{x} + M_{21}\ddot{\theta}_1 + M_{22}\ddot{\theta}_2 + K_2(\theta_1, \theta_2, \dot{\theta}_2) + G_2 = \tau_1 \tag{A.20}$$

$$H_{31}\ddot{x} + M_{31}\ddot{\theta}_1 + M_{32}\ddot{\theta}_2 + K_3(\theta_1, \dot{\theta}_1, \theta_2) + G_3 = \tau_2 \tag{A.21}$$

$$H_{11} = -(m_0 + m_1 + m_2) \qquad M_{11} = (l_1m_2 + l_{1cm}m_1)cos(\theta_1) \qquad M_{12} = l_{2cm}m_2cos(\theta_2)$$
$$H_{21} = M_{11} \qquad M_{21} = -(l_1^2m_2 + l_{1cm}^2m_1 + I_1) \qquad M_{22} = -l_1l_{2cm}m_2cos(\theta_1 - \theta_2)$$
$$H_{31} = M_{12} \qquad M_{31} = M_{22} \qquad M_{32} = -(l_{2cm}^2m_2 + I_2)$$
$$G_2 = (l_1m_2 + l_{1cm}m_1)sin(\theta_1)g \qquad G_3 = m_2l_{2cm}sin(\theta_2)g$$

$$K_1 = -(l_1m_2 + l_{1cm}m_2)sin(\theta_1)\dot{\theta}_1^2 - l_{2cm}m_2sin(\theta_2)\dot{\theta}_2^2$$
$$K_2 = -l_1l_{2cm}m_2sin(\theta_1 - \theta_2)\dot{\theta}_2^2$$
$$K_3 = l_1l_{2cm}m_2sin(\theta_1 - \theta_2)\dot{\theta}_1^2$$

For now the focus is on finding an expression for the two angular accelerations $\ddot{\theta}_1$ and $\ddot{\theta}_2$ leaving the horizontal acceleration $\ddot{x}$ for later when the motor system and the pendulum system are combined.
By rearranging Equations A.20-A.21 and inserting the expression in for τ_1 and τ_2 the two equations can simultaneously solved as shown below.

$$\begin{aligned} M_{21}\ddot{\theta}_1 + M_{22}\ddot{\theta}_2 &= K_{v1}\dot{\theta}_1 + K_{d1}M_{d1} - H_{21}\ddot{x} - K_2 - G_2 \\ f_{11}\ddot{\theta}_1 + f_{12}\ddot{\theta}_2 &= f_{13} \end{aligned}$$

$$\begin{aligned} M_{31}\ddot{\theta}_1 + M_{32}\ddot{\theta}_2 &= K_{v2}\dot{\theta}_2 + K_{d2}M_{d2} - H_{31}\ddot{x} - K_3 - G_3 \\ f_{21}\ddot{\theta}_1 + f_{22}\ddot{\theta}_2 &= f_{23} \end{aligned}$$

$$\ddot{\theta}_1 = \frac{f_{13}f_{22} - f_{12}f_{23}}{f_{22}f_{11} - f_{21}f_{12}} \tag{A.22}$$

$$\ddot{\theta}_2 = \frac{f_{23}f_{11} - f_{21}f_{13}}{f_{22}f_{11} - f_{21}f_{12}} \tag{A.23}$$

$$\ddot{\theta}_1 = \frac{(K_{v1}\dot{\theta}_1 + K_{d1}M_{d1} - H_{21}\ddot{x} - K_2 - G_2)M_{32} - M_{22}(K_{v2}\dot{\theta}_2 + K_{d2}M_{d2} - H_{31}\ddot{x} - K_3 - G_3)}{M_{32}M_{21} - M_{31}M_{22}} \tag{A.24}$$

$$\ddot{\theta}_2 = \frac{(K_{v2}\dot{\theta}_2 + K_{d2}M_{d2} - H_{31}\ddot{x} - K_3 - G_3)M_{21} - M_{31}(K_{v1}\dot{\theta}_1 + K_{d1}M_{d1} - H_{21}\ddot{x} - K_2 - G_2)}{M_{32}M_{21} - M_{31}M_{22}} \tag{A.25}$$

Equations A.24-A.25 are the dynamic equations for the angular accelerations. Even tough they are already quite complex lets conclude this part by writing them down in detail.

$$\begin{aligned} \ddot{\theta}_1 = \frac{1}{Den}&(l_1 l_{2cm} m_2 cos(\theta_1 - \theta_2)(K_{v2}\dot{\theta}_2 - l_{2cm}m_2 cos(\theta_2)\ddot{x} + K_{d2}M_{d2} - l_{2cm}m_2 sin(\theta_2)g \\ &- l_1 l_{2cm} m_2 sin(\theta_1 - \theta_2)\dot{\theta}_1^2) + (-l_{2cm}^2 m_2 - I_2)(-(l_1 m_2 + l_{1cm}m_1)cos(\theta_1)\ddot{x} \\ &+ K_{v1}\dot{\theta}_1 + K_{d1}M_{d1} - (l_1 m_2 + l_{1cm}m_1)sin(\theta_1)g + l_1 l_{2cm} m_2 sin(\theta_1 - \theta_2)\dot{\theta}_2^2)) \end{aligned} \tag{A.26}$$

$$\ddot{\theta}_2 = \frac{1}{Den}((-l_1^2 m_2 - l_{1cm}^2 m_1 - I_1)(K_{v2}\dot{\theta}_2 - l_{2cm} m_2 cos(\theta_2)\ddot{x} + K_{d2} M_{d2} - l_{2cm} m_2 sin(\theta_2) g$$
$$- l_1 l_{2cm} m_2 sin(\theta_1 - \theta_2)\dot{\theta}_1^2) + l_1 l_{2cm} m_2 cos(\theta_1 - \theta_2)(-(l_1 m_2 + l_{1cm} m_1) cos(\theta_1)\ddot{x} \quad \text{(A.27)}$$
$$+ K_{v1}\dot{\theta}_1 + K_{d1} M_{d1} - (l_1 m_2 + l_{1cm} m_1) sin(\theta_1) g + l_1 l_{2cm} m_2 sin(\theta_1 - \theta_2)\dot{\theta}_2^2))$$

$$Den = (l_1^2 m_2 + l_{1cm}^2 m_1 + I_1)(l_{2cm}^2 m_2 + I_2) - cos(\theta_1 - \theta_2)^2 l_1^2 l_{2cm}^2 m_2^2 \quad \text{(A.28)}$$

A.1.2 Motor system

A block diagram of the motor with a tacho-feedback is shown in Figure A.2.

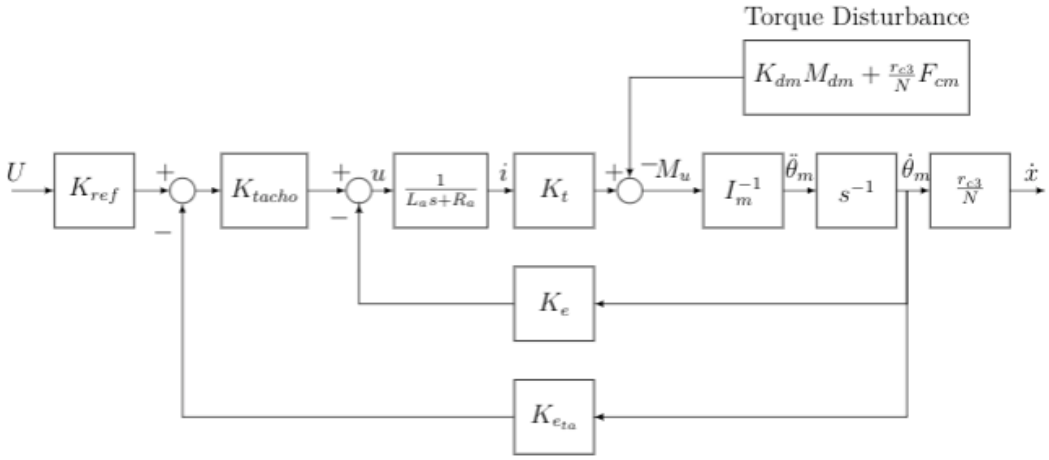

Figure A.2: The motor Block-Diagram.

The required differential equations that describe this part of the system are derived from the block diagram above. The voltage applied to the motor is expressed as

$$u = K_{ref} K_{tacho} U - (K_e + K_{e_{ta}} K_{tacho})\dot{\theta}_m \quad \text{(A.29)}$$

where U is the control voltage for the motor. We also have a relationship between the terminal voltage and the current running trough the motor.

$$u = L_a \dot{i} + R_a i \quad \text{(A.30)}$$

Now combining and rearranging EquationA.29-A.30 we have a differential equation describing the current.

$$\dot{i} = -\frac{(K_e + K_{e_{ta}} K_{tacho})}{La}\dot{\theta}_m - \frac{R_a}{L_a} i + \frac{K_{ref} K_{tacho}}{L_a} U \tag{A.31}$$

Since we are aiming towards integrating the pendulum system and the motor system it's convenient to define a factor for converting angular dynamics of the motor shaft to the linear dynamics of the cart. In EquationA.32 N stands for the gear ratio and r_{c3} is the radius of the cog wheel.

$$x = \frac{r_{c3}}{N}\theta_m \tag{A.32}$$

If we rewrite EquationA.31 using the relationship in EquationA.32 we get,

$$\dot{i} = -\frac{N}{r_{c3}}\frac{(K_e + K_{e_{ta}} K_{tacho})}{L_a}\dot{x} - \frac{R_a}{L_a} i + \frac{K_{ref} K_{tacho}}{L_a} U \tag{A.33}$$

Now taking a look at the motor torque M_u. As seen from Fig.A.2, the torque is a function of the current i and the disturbances from the Coulomb friction M_{dm} and the force F_p form the pendulum system.

$$M_u = K_t i - (K_{dm} M_{dm} + \frac{r_{c3}}{N} F_p) \tag{A.34}$$

$$I_m \ddot{\theta}_m = K_t i - (K_{dm} M_{dm} + \frac{r_{c3}}{N} F_p) \tag{A.35}$$

$$\ddot{x} = \frac{r_{c3}}{N I_m} K_t i - \frac{r_{c3}}{N I_m} K_{dm} M_{dm} - \frac{r_{c3}^2}{N^2 I_m} F_p \tag{A.36}$$

A.1.3 Overall system

Now a set of differential equations have been derived that describe the overall system. F_p appears in both systems and can be used to combine the two systems. First Equations A.24-A.25 are inserted into Equation A.19 which gives,

$$F_p = H_{11}\ddot{x} + M_{11}\left(\frac{f_{13} M_{32} - M_{22} f_{23}}{M_{32} M_{21} - M_{31} M_{22}}\right) + M_{12}\left(\frac{f_{23} M_{21} - M_{31} f_{13}}{M_{32} M_{21} - M_{31} M_{22}}\right) + K1 \tag{A.37}$$

$$f_{13} = (K_{v1}\dot{\theta}_1 + K_{d1} M_{d1} - H_{21}\ddot{x} - K_2 - G_2)$$
$$f_{23} = (K_{v2}\dot{\theta}_2 + K_{d2} M_{d2} - H_{31}\ddot{x} - K_3 - G_3)$$

Isolating $\ddot{x}$, which is embedded in f_{13} and f_{23} in Equation A.37 gives,

$$\begin{aligned} F_p =& \left(H_{11} + M_{11}\left[\frac{M_{22}H_{31} - M_{32}H_{21}}{M_{32}M_{21} - M_{31}M_{22}}\right] + M_{12}\left[\frac{M_{31}H_{21} - M_{21}H_{31}}{M_{32}M_{21} - M_{31}M_{22}}\right]\right)\ddot{x} \\ &+ M_{11}\left[\frac{\bar{f}_{13}M_{32} - M_{22}\bar{f}_{23}}{M_{32}M_{21} - M_{31}M_{22}}\right] + M_{12}\left[\frac{\bar{f}_{23}M_{21} - M_{31}\bar{f}_{13}}{M_{32}M_{21} - M_{31}M_{22}}\right] + K1 \end{aligned} \tag{A.38}$$

$$\begin{aligned} \bar{f}_{13} &= (K_{v1}\dot{\theta}_1 + K_{d1}M_{d1} - K_2 - G_2) \\ \bar{f}_{23} &= (K_{v2}\dot{\theta}_2 + K_{d2}M_{d2} - K_3 - G_3) \end{aligned}$$

Now we are ready to combine the two systems by inserting F_p into Equation A.36. Collecting all the $\ddot{x}$ terms to the left side of the equation and calling it $\bar{D}$ and leaving the reminder of F_p on the right side and renaming it $\bar{F}_p$

$$\bar{D}\ddot{x} = \frac{r_{c3}}{NI_m}K_t i - \frac{r_{c3}}{NI_m}K_{dm}M_{dm} - \frac{r_{c3}^2}{N^2 I_m}\bar{F}_p \tag{A.39}$$

where

$$\bar{F}_p = \left(M_{11}\left[\frac{\bar{f}_{13}M_{32} - M_{22}\bar{f}_{23}}{M_{32}M_{21} - M_{31}M_{22}}\right] + M_{12}\left[\frac{\bar{f}_{23}M_{21} - M_{31}\bar{f}_{13}}{M_{32}M_{21} - M_{31}M_{22}}\right] + K1\right) \tag{A.40}$$

and

$$\bar{D} = 1 + \frac{r_{c3}^2}{N^2 I_m}\left(H_{11} + M_{11}\left[\frac{M_{22}H_{31} - M_{32}H_{21}}{M_{32}M_{21} - M_{31}M_{22}}\right] + M_{12}\left[\frac{M_{31}H_{21} - M_{21}H_{31}}{M_{32}M_{21} - M_{31}M_{22}}\right]\right) \tag{A.41}$$

Finally, to conclude this chapter, let's collect all the differential equations that describe the overall system.

$$\ddot{x} = \bar{D}^{-1}\left[\frac{r_{c3}}{NI_m}K_t i - \frac{r_{c3}}{NI_m}K_{dm}M_{dm} - \frac{r_{c3}^2}{N^2 I_m}\bar{F}_p\right] \tag{A.42}$$

$$\ddot{\theta}_1 = \frac{(K_{v1}\dot{\theta}_1 + K_{d1}M_{d1} - H_{21}\ddot{x} - K_2 - G_2)M_{32} - M_{22}(K_{v2}\dot{\theta}_2 + K_{d2}M_{d2} - H_{31}\ddot{x} - K_3 - G_3)}{M_{32}M_{21} - M_{31}M_{22}} \tag{A.43}$$

$$\ddot{\theta}_2 = \frac{(K_{v2}\dot{\theta}_2 + K_{d2}M_{d2} - H_{31}\ddot{x} - K_3 - G_3)M_{21} - M_{31}(K_{v1}\dot{\theta}_1 + K_{d1}M_{d1} - H_{21}\ddot{x} - K_2 - G_2)}{M_{32}M_{21} - M_{31}M_{22}} \tag{A.44}$$

$$\dot{i} = -\frac{N(K_e + K_{eta}K_{tacho})}{r_{c3}L_a}\dot{x} - \frac{R_a}{L_a}i + \frac{K_{ref}K_{tacho}}{L_a}U \tag{A.45}$$

APPENDIX B

Numerical Values

Table B.1: List of variables and numerical values of constants for the cart.

Cart:	Symbol	Description	Value
	F_{cm}	Force exerted on cart by motor system	
	x	Cart position	
	$\dot{x}$	Cart velocity	
	$\ddot{x}$	Cart acceleration	
	n_x	Measurements noise	
	K_{nx}	Noise scale constant	$5.0e^{-4}$
	M_0	Mass of cart	$0.84Kg$

Table B.2: List of variables and numerical values of constants for the lower arm.

Lower Arm:	Symbol	Description	Value
	θ_1	Angle with respect to vertical	
	$\dot{\theta}_1$	Angular velocity	
	$\ddot{\theta}_1$	Angular acceleration	
	M_{d1}	Coulomb friction disturbance (direction)	{-1,1}
	K_{d1}	Disturbance scale constant	$4.0e^{-4}N$
	n_1	Measurement noise	
	K_{n1}	Noise scale constant	$1.6e^{-3}N$
	M_1	Mass of arm	$0.584Kg$
	I_1	Inertia around lower joint	$2.678e^{-2}Kgm^2$
	l_1	Length of arm	$0.535m$
	l_{1cm}	Length from lower joint to center of mass	$0.355m$

Table B.3: List of variables and numerical values of constants for the upper arm.

Upper Arm:	Symbol	Description	Value
	θ_2	Angle with respect to vertical	
	$\dot{\theta}_2$	Angular velocity	
	$\ddot{\theta}_2$	Angular acceleration	
	θ_3	Angle between lower and upper arm	
	M_{d2}	Coulomb friction disturbance (direction)	{-1,1}
	K_{d2}	Disturbance scale constant	$4.0e^{-4}N$
	n_3	Measurement noise in θ_3	
	K_{n3}	Noise scale constant	$1.6e^{-3}N$
	M_2	Mass of arm	$0.21Kg$
	I_2	Inertia around lower joint	$5.217e^{-3}Kgm^2$
	l_{2cm}	Length from upper joint to center of mass	$0.12m$

Inertia of the belt drive:

$$I_c = \frac{1}{2}(M_{c1}r_{c1}^2 + \frac{1}{N^2}(M_{c2}r_{c2}^2 + 2M_{c3}r_{c3}^2 + 2M_{axle}r_{axle}^2)) \tag{B.1}$$

Inertia seen from motor axis:

$$I_m = I_{rm} + I_c \tag{B.2}$$

Table B.4: List of variables and numerical values of constants for the motor system.

Motor:	Symbol	Description	Value
	θ_m	Rotor angle	
	$\dot{\theta}_m$	Angular velocity	
	$\ddot{\theta}_m$	Angular acceleration	
	M_{dm}	Torque disturbance (direction)	{-1,1}
	K_{dm}	Disturbance scale constant	$6.06e^{-2}N$
	i	Motor current	
	u	Motor terminal voltage	
	U	Control signal (voltage)	
	I_m	Inertia seen from motor axis	
	I_{rm}	Rotor inertia	$64.7e^{-7}Kgm^2$
	L_a	Rotor inductance	$65e^{-6}H$
	R_a	Terminal resitance	0.5Ω
	K_e	Motor back EMF	$21.44e^{-3}\frac{V}{(rad/sec)}$
	$K_{e_{ta}}$	Tacho EMF	$41.06e^{-3}\frac{V}{(rad/sec)}$
	K_t	Torque constant	$21.44e^{-3}\frac{Nm}{A}$
	K_{ref}	Torque constant	1
	K_{tacho}	Tacho gain constant	60
	M_{axle}	Mass of axle	$0.1kg$
	M_{c1}	Mass of cog wheel 1	$5.3e^{-3}kg$
	M_{c2}	Mass of cog wheel 2	$0.1kg$
	M_{c3}	Mass of cog wheel 3	$0.675kg$
	r_{axle}	radius of axle	$5e^{-3}m$
	r_{c1}	radius of cog wheel 1	$5.3e^{-3}m$
	r_{c2}	radius of cog wheel 2	$28.27e^{-3}m$
	r_{c3}	radius of cog wheel 3	$30.32e^{-3}m$
	N	Gear constant	5

APPENDIX C

Test-Rig Electronics

Prior to this project the author upgraded the electronics of the Test-Rig. The electronics were in bad shape as many wires were longer then needed, little care taken to minimize cross-talk between wires and some critical ground connections were missing. Also the inconsistent color-code of the wires did not help when trouble-shooting the circuit. So it was decided to re-wire the system completely.
The systems electronics can be divided into two subsystems, a sensor-circuit and a motor-circuit. The system also has a three-loop relay that servers as a start/stop switch and as an emergency break switch if the car reaches either end of the track. List of most important electronics devices can be found in Table C.1. With regards to this project it should be noted that according the data-sheet the maximum peak current of the amplifier is 12A and maximum continuous current is 6A.

Table C.1: List of main electronics components of the Test-Rig along with basic information about each device.

DC Motor	Faulhaber	3557-012CR	80 mNm
Motor Amplifier	Advanced Motion Controls	Analog Servo Drive	12A8
AD/DA converter	National Instruments	NI 6251	16bit
Relay	Kuhnke	-	-

C.1 Sensor circuit

The sensor circuit has three potentiometers, an amplifier and offset-adjustment. Two potentiometers are used to measure the joint angles of the pendulum, and the third potentiometer is used to measure the position of the car that moves vertically along its track.

It is desired that when the arms of the pendulum are perfectly vertical the measured joint angles should amount to 0V. In order to calibrate this parameter the pendulum was turned up side down, making sure the frame was as close to horizontal as possible, leaving the pendulum to hang freely creating a 90° angle between the track and the arms of the pendulum. With the pendulum in this orientation the offset was adjusted so that vertical pendulum gives 0V. Then the gain of the amplifier was set such that clockwise and counter-clockwise extremes give $\pm 5V$ respectively for both top and bottom joint. If the need arises it is easy to increase the voltage range to $\pm 10V$, but for now the $\pm 5V$

range is acceptable.
Figure C.1 shows the amplifier circuit diagram for the bottom joint sensor. The circuit for the top joint sensor is identical, how ever the amplifier gain and offset might have different values.

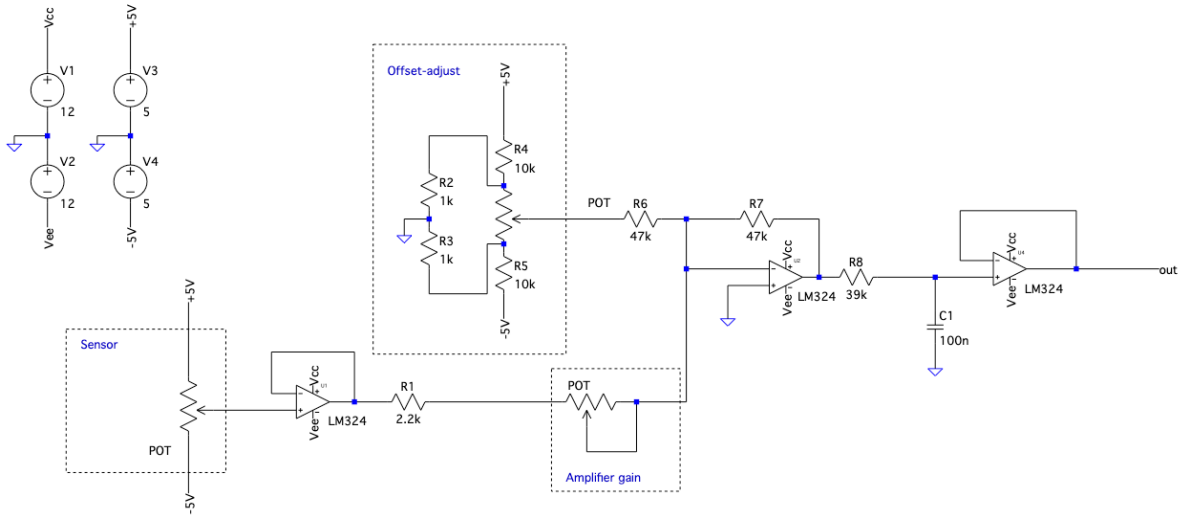

Figure C.1: Amplifier circuit for bottom joint sensor.

The cart position sensor circuit can be seen in Figure C.2. It is a simple buffer circuit with a passive RC-filter, but no amplification of the signal is available.

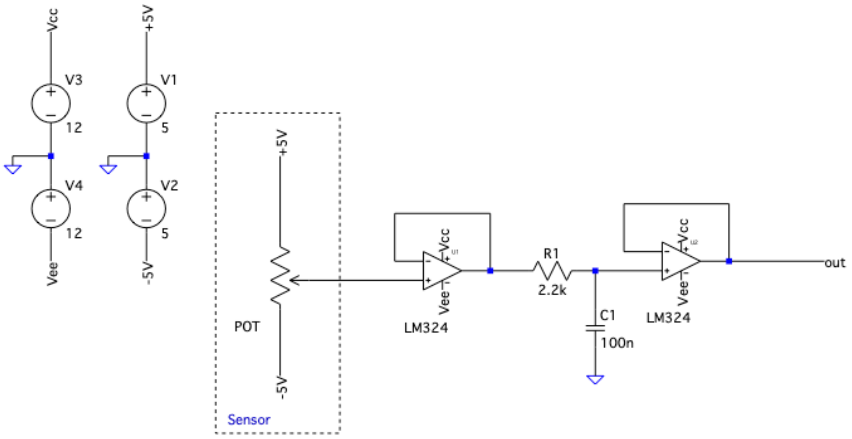

Figure C.2: Circuit for car position measurements.

Figure C.3 shows the apparent noise on all sensors in the upgraded system. It shows that the noise amplitude is pretty much the same in all circuits. This amount of noise is considered not to be a problem since 1.2mV noise amplitude translates roughly into 0.02° offset in the angle measurements.

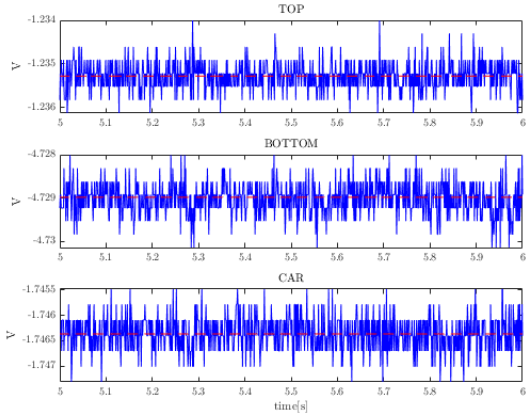

Figure C.3: Sensor noise in the upgraded system.

C.2 Motor circuit

The other electronic subsystem of the pendulum is the motor-circuit. It mainly consists of a DC motor, pulse width modulation amplifier and a relay switch. The relay has three loops but only two loops are used.
First loop a is circuit for emergency breaks and startup. As can be seen in Figure C.4, 10V are applied to the system. The emergency breaks EB1 and EB2 are normally closed switches that break the circuit if the car reaches either end if the track. If the normally open push-button PB1 is closed, node A is energized and the relay flips its switches activating the loops.

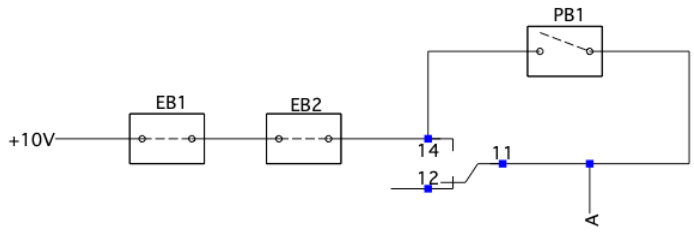

Figure C.4: Start up and emergency break loop. PB1 is a push-button used for start up, EB! and EB2 are the emergency break circuit brakers.

Like stated before the upgraded version of the system uses only two of the three loops available in the relay. In the upgraded version seen in Figure C.5 the control signal goes directly to the amplifier, bypassing the relay. This new configuration reduces the length of wires, shortening the control signal path which minimizes the effect of noise in the signal and other disturbances that might be introduced by the relay.

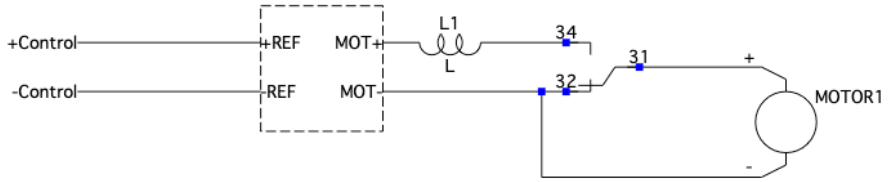

Figure C.5: Upgraded Motor loop, the dashed box represents the amplifier.

APPENDIX D

Matlab and simulink

D.1 Block diagrams

The simulink model is originates from the previous work of [Pou01].However it has been slightly modified as a current limiter has been added to the motor system, offsets applied to the angle measurements and the three simulation stop conditions. The simulink model and the most relevant matlab files are handed in with the project.

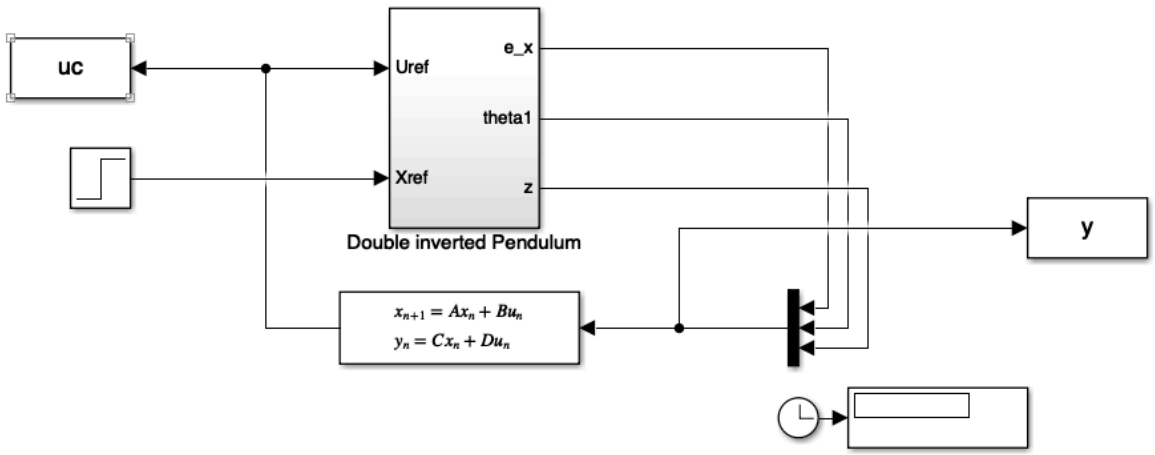

Figure D.1: Full system simulink block diagram.

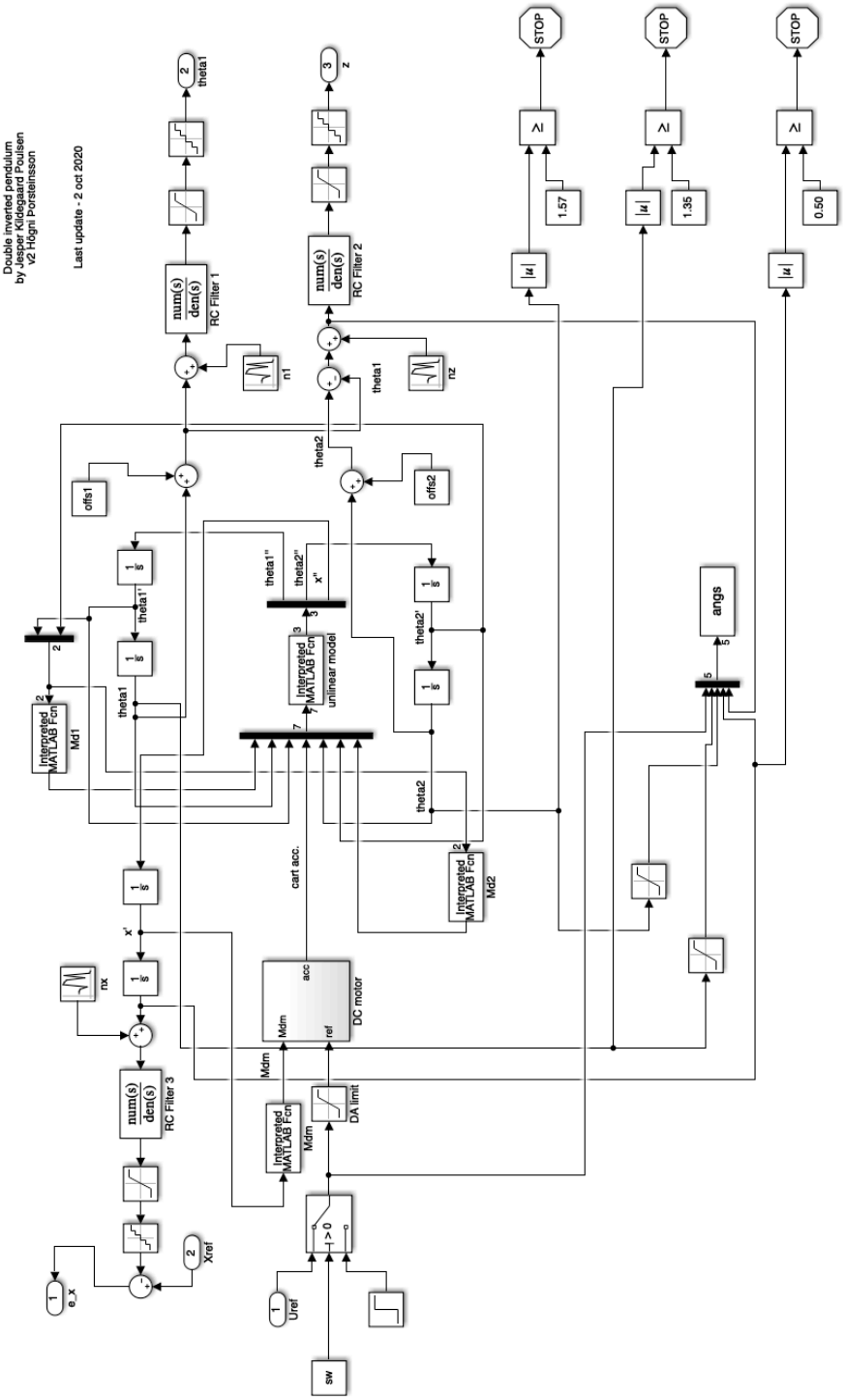

Figure D.2: Double Inverted pendulum simulink sub-system.

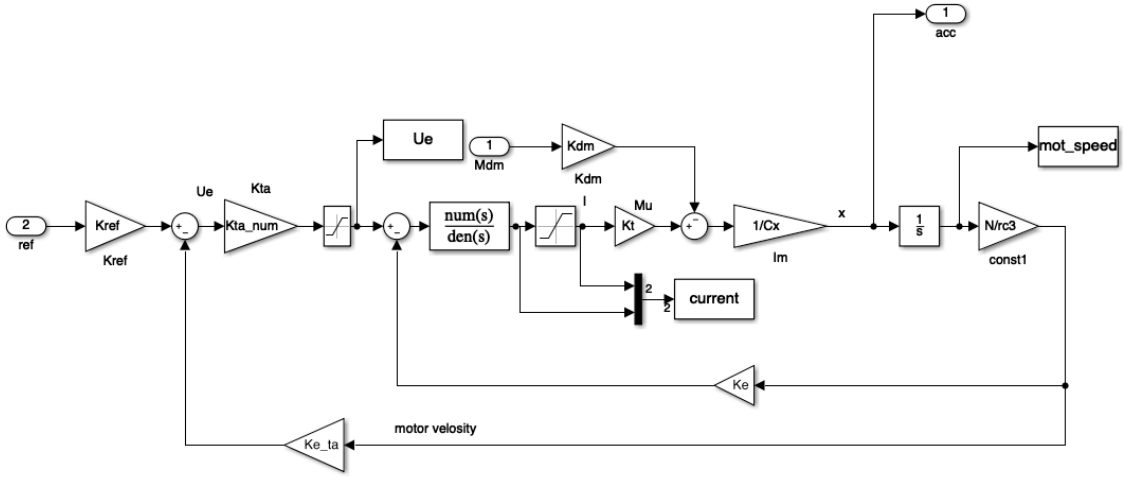

Figure D.3: DC-motor simulink sub-system.

D.2 Functions

D.2.1 Nonlinear Pendulum

```
%*******************************************************************
%Defines the unlinear pendulm system
%
%*******************************************************************
%function y=unlin_tf(u)
function y=nonlin_dip(u)
global K_f12 K1_f13 Kv1 K2_f13 K3_f13 Kd1 Kd2 K_f21 K1_f23 Kv2 K2_f23 K3_f23 f11 f
global M1 M2 l1 l1_cm l2_cm g Cx N rc3 I1 I2;
%*******************************************************************
%Unlinear system constants
%
%theta1''=(f13*f22-f23*f12)/(f11*f22-f21*f12)
%theta2''=(f11*f23-f21*f13)/(f11*f22-f21*f12)
%
%*******************************************************************
K_f12 = M2*l2_cm*l1;
K1_f13 = M2*l2_cm*l1;
K2_f13 = -(M2*l1+M1*l1_cm);
K3_f13 = (M1*l1_cm+M2*l1)*g;
```

```
K_f21 = M2*l1*l2_cm;
K1_f23 = -M2*l1*l2_cm;
K2_f23 = -M2*l2_cm;
K3_f23 = M2*l2_cm*g;

f11=I1+M1*l1_cm^2+M2*l1^2;
f22=(I2+M2*(l2_cm^2));

Km1 = (rc3*(M1*l1_cm*cos(u(2))+M2*l1*cos(u(2))))/(Cx*N);
Km2 = (rc3*(M2*l2_cm*cos(u(5))))/(Cx*N);
Km3 = (rc3*(-M1*l1_cm*sin(u(2))-M2*l1*sin(u(2))))/(Cx*N);
Km4 = (rc3*(-M2*l2_cm*sin(u(5))))/(Cx*N);

f12 = K_f12*cos(u(5)-u(2));
f13 = -Kv1*u(3)...
  +K1_f13*sin(u(5)-u(2))*u(6)*u(6)...
  +K3_f13*sin(u(2))-Kd1*u(1);

Cx1 = K2_f13*cos(u(2));

f21=K_f21*cos(u(5)-u(2));
f23=K1_f23*sin(u(5)-u(2))*u(3)*u(3)...
  -Kv2*u(6)...
  +K3_f23*sin(u(5))-Kd2*u(7);

Cx2 = K2_f23*cos(u(5));

%denuminator for angle acc. functions
den = f11*f22-f21*f12;

xdd =  (u(4)-Km1*((f13*f22-f23*f12)/den)-Km2*((f11*f23-f21*f13)/den)-Km3*u(3)*u(3)-Km4*
%FX1 = ((Cx1*f22-Cx2*f12))
%FX2 = ((Cx2*f11-Cx1*f21))

%angle acceleration.
y(1)=((f13+Cx1*xdd)*f22-(f23+Cx2*xdd)*f12)/den;
y(2)=(f11*(f23+Cx2*xdd)-f21*(f13+Cx1*xdd))/den;
%linear acceleration.
y(3)=xdd;
```

D.2.2 Friction functions

```
%
% Defines the Coulomb friction for joint 1
%
function y=md1(u1,u2)
    y=sign(u1)-sign(u2-u1);
end


%
% Defines the Coulomb friction for joint 2
%
function y=md2(u1,u2)
    y=sign(u1-u2);
end


%
% Defines direction of rotor friction
%
function y=mdm(u)
    y=sign(u(1));
end
```

APPENDIX E

Control algorithm in software

The 7 step implementation of controller in state space form as described in Chapter 6.5. Note that here step 4 (send control signal) is executed last. This is not considered an issue since the time period from step 3 to step 6 is relatively small. The full program is included in the project hand-in.

```
double DIP_control()
{
    int i,j;
    double tmp1,UO,DUMMY;
    tmp1 = 0;
    DUMMY = 0;
    // 1.
    for(j = 0; j < C_COL; j++)
    {
        tmp1 = C->data[0][j]*X[j];
        DUMMY = tmp1+DUMMY;
    }
    tmp1 = 0;
    // 2. GET ERROR
    E[0] = ref-car_value;
    E[1] = th1;
    E[2] = th3;
    // 3.
    for(j = 0; j<D_COL; j++)
    {
        tmp1 = tmp1 + D->data[0][j]*E[j];
    }
    UO = DUMMY+tmp1;
    // 4. RETURN UO
    // 5.
    for(i = 0; i<A_ROWS;i++)
    {
```

```
        tmp1 = 0;
        for(j = 0; j<A_COL;j++)
        {
            W[i]= W[i]+A->data[i][j]*X[j];
        }
    }
        // 6
    for(i = 0; i<B_ROWS;i++)
    {
        tmp1 = 0;
        for(j = 0; j<B_COL;j++)
        {
            tmp1 = tmp1 + B->data[i][j]*E[j];
        }
        X[i] = W[i]+tmp1;
        // 7.
        W[i] = 0.0;
     }
    tmp1 = 0;

    return UO;
}
```

Bibliography

[DB17] Richard C Dorf and Robert H. Bishop. *Modern Control System*. 13th edition. Pearson Education, 2017. ISBN: 9781292152974.

[ES08] Ole Jannerup Elbert Hendricks and Paul Haase Sørensen. *Linear System Control*. First Edition. Springer-Verlag, 2008. ISBN: 9783540784852.

[Lut97] Jim Luther. *The double inverted pendulum*. M.Sc Thesis. Departement of Automation, DTU, 1997.

[MLL82] M.L.Levin. *Datamatbaserede Reguleringssystemer*. Servolaboratoriet, 1982.

[NV13] Zdenék Neusser and Michael Valásek. *Control of the Double Inverted Pendulum on a Cart using the Natural Motion*. Acta Polytechnica. Czech Technical University, January 2013. URL: https://doi.org/10.14311/AP.2013.53.0883.

[Pou01] Jesper Kildegaard Poulsen. *Modelling and Control of unstable System*. M.Sc Thesis. Department of Automation, DTU, January 2001.

[Sch] David Schleef. *Comedi - Linux Control and Measurement Device Interface*. URL: https://www.comedi.org/.

[SP05] Sigurd Skogestad and Ian Postlethwaite. *Multivariable Feedback Control*. Second Edition. John Wiley Sons Ltd, 2005. ISBN: 9780470011676.

[SP19] Sondarangallage DA Senjeewa and Manukid Parnichkun. *Control of Rotary Double Inverted Pendulum system using mixed sensitivity H-inf controller*. International Journal of Advanced Robotic Systems. April 2019. URL: https://journals.sagepub.com/doi/full/10.1177/1729881419833273.

[ZR01] Wei Zong and Helmut Röck. *Energy and passivity based control of the double inverted pendulum on a cart*. Proceedings of the 2001 IEEE International conference of Control Applications. Christian-Albrechts-University of Kiel, September 2001.

DTU Electrical Engineering
Department of Electrical Engineering
Technical University of Denmark

Ørsteds Plads
Building 348
DK-2800 Kgs. Lyngby
Denmark
Tel: (+45) 45 25 38 00

www.elektro.dtu.dk